High and asymmetric somato-dendritic coupling of V1 layer 5 neurons independent of visual stimulation and locomotion

Valerio Francioni[1, 2], Zahid Padamsey[1], and Nathalie L. Rochefort[1, 2, †]

[1]Centre for Discovery Brain Sciences, School of Biomedical Sciences Edinburgh, Edinburgh, EH8 9XD, United Kingdom.

[2]Simons Initiative for the Developing Brain, University of Edinburgh, Edinburgh, EH8 9XD, United Kingdom.

[†] Corresponding Author:
Nathalie Rochefort
Centre for Discovery Brain Sciences, Biomedical Sciences Edinburgh, Edinburgh, EH8 9XD, United Kingdom.
n.rochefort@ed.ac.uk

Abstract

Active dendrites impact sensory processing and behaviour. However, it remains unclear how active dendritic integration relates to somatic output *in vivo*. We imaged semi-simultaneously GCaMP6s signals in the soma, trunk and distal tuft dendrites of layer 5 pyramidal neurons in the awake mouse primary visual cortex. We found that apical tuft signals were dominated by widespread, highly correlated calcium transients throughout the tuft. While these signals were highly coupled to trunk and somatic transients, the frequency of calcium transients was found to decrease in a distance-dependent manner from soma to tuft. *Ex vivo* recordings suggest that low-frequency back-propagating action potentials underlie the distance-dependent loss of signals, while coupled somato-dendritic signals can be triggered by high-frequency somatic bursts or strong apical tuft depolarization. Visual stimulation and locomotion increased neuronal activity without affecting somato-dendritic coupling. High, asymmetric somato-dendritic coupling is therefore a widespread feature of layer 5 neurons activity *in vivo*.

Introduction

Active dendritic conductances impact the integration of synaptic inputs and its effect on somatic output (Grienberger, Chen and Konnerth, 2015; Stuart and Spruston, 2015). Different types of active dendritic currents have been described to support local nonlinear events, primarily driven by NMDA- and voltage-gated conductances (Schiller *et al.*, 1997; Matthew E. Larkum, Zhu and Sakmann, 1999). In cortical layer 5 excitatory neurons, nonlinear dendritic spikes have been reported in the long apical dendrite and tuft, both *in vitro* and *in vivo* (Grienberger, Chen and Konnerth, 2015; Stuart and Spruston, 2015). These dendritic events are generally associated with calcium influx both locally and globally in the apical tuft (Xu *et al.*, 2012; Hill *et al.*, 2013; Palmer *et al.*, 2014; Cichon and Gan, 2015; Manita *et al.*, 2015; Takahashi *et al.*, 2016). Additionally, the coincident occurrence of back-propagating action potentials and tuft depolarization was shown to generate widespread calcium transients in the apical tuft dendrites (Spruston *et al.*, 1995; Magee and Johnston, 1997; Svoboda *et al.*, 1997; Helmchen *et al.*, 1999; Larkum, Zhu and Sakmann, 1999; Waters *et al.*, 2003; Manita *et al.*, 2015) .

The frequency and dynamics of local dendritic nonlinearities *in vivo* have been a matter of debate. Events described as local dendritically-generated spikes were reported in layer 2/3 neurons of the visual and somatosensory cortex during sensory stimulation (Smith *et al.*, 2013; Palmer *et al.*, 2014). In the visual cortex, it has been suggested that dendritic spikes triggered by visual input enhance somatic tuning to the preferred orientation (Smith *et al.*, 2013). However, single dendrite recordings prevented conclusions about the spatial extent and the branch-specific nature of the detected events. Using calcium imaging in the mouse motor cortex, one study suggested that individual branches of densely labelled layer 5 neurons selectively display local calcium transients correlated with specific motor outputs (Cichon and Gan, 2015). However, other studies reported prevalent global calcium signals throughout layer 5 apical tuft dendrites in the barrel and motor cortex (Xu *et al.*, 2012; Hill *et al.*, 2013). While layer 5 apical dendritic calcium transients were shown to correlate with behaviourally relevant features (Xu *et al.*, 2012; Takahashi *et al.*, 2016; Peters *et al.*, 2017; Kerlin *et al.*, 2018; Ranganathan *et al.*, 2018), the coupling between apical tuft activity and somatic output remains poorly understood.

By using semi-simultaneous imaging of apical trunk and somatic GCaMP6f signals in layer 5 neurons, a recent study has shown that apical trunk dendritic calcium signals were highly correlated with somatic signals in the primary visual cortex (V1) of awake behaving mice (Beaulieu-Laroche *et al.*, 2019). Layer 5 pyramidal neurons in V1 display selective responses to physical features of visual stimuli, such as the orientation and direction of movement (Niell and Stryker, 2008; Kim *et al.*, 2015) and their activity is modulated by locomotion (Erisken *et al.*, 2014; Dadarlat and Stryker, 2017; Pakan, Francioni and Rochefort, 2018). However, Beaulieu-Laroche et al. (2019) found that neither visual stimulation nor locomotion altered the high somato-dendritic coupling of calcium transients.

Here, we used a similar approach to image GCaMP6s calcium signals in the soma, trunk and distal tuft dendrites of layer 5 pyramidal neurons, both in darkness and during the presentation of drifting gratings, while head-fixed mice were either running or stationary. In agreement with Beaulieu-Laroche et al. (2019), we found that the apical trunk dendritic calcium signals were highly correlated with somatic signals. We extended these results by showing that the whole apical tuft was highly correlated to trunk activity; the vast majority of dendritic calcium transients in the apical tuft were coincident with global events, with rare cases of branch-specific activity, limited to the smallest amplitude events. In addition, by imaging somatic and dendritic GCaMP6s signals, we found that somato-dendritic coupling was asymmetric; while almost all events observed in the tuft were also visible in the soma, around 40% of somatic events attenuated in an amplitude and distance-dependent manner from the soma to the apical tuft. *Ex vivo* recordings of GCaMP6s signals suggested that coupled somato-dendritic events likely reflected either strong apical tuft inputs or high frequency somatic activity, whereas attenuated events were likely caused by low frequency back-propagating action potentials. We compared GCaMP6s with GCaMP6f signals and showed that due to a reduced sensitivity, attenuation of events from soma to dendrite were underestimated with GCaMP6f (Beaulieu-Laroche *et al.*, 2019). Finally, our results show that neither visual stimulation nor locomotion affected the *in vivo* coupling of somatic and apical tuft calcium signals.

Results

Highly correlated, widespread calcium signals in apical tuft dendrites of single layer 5 neurons

We imaged changes in fluorescence over time in apical dendrites of individual layer 5 pyramidal neurons sparsely labelled with either the calcium sensor GCaMP6s or GCaMP6f (Chen *et al.*, 2013) in the primary visual cortex of adult mice. Using single-plane two-photon imaging (at 120 Hz), we first monitored changes of GCaMP6f signals in individual apical tuft dendrites of head-fixed, awake behaving mice that were free to run on a cylindrical treadmill (Figure 1A). Our results showed highly correlated calcium signals in all apical dendritic branches belonging to the same neuron and imaged in a given field of view (Pearson's correlation coefficient r = 0.92, SEM = 0.01, n = 25 fields of view recorded from 14 neurons, 6 animals) (Figure 1B, 1C, 1D). Given that electrical signals are known to attenuate in a distant dependent manner, we tested whether the correlation of calcium transients between apical tuft branches decreased with distance from the apical trunk (nexus). We reconstructed each individual neuron for which we imaged the apical tuft and quantified the correlation of fluorescence signals across sibling branches. We found that calcium signals in sibling branches were highly correlated (average Pearson's correlation coefficient r = 0.92) regardless of their branching order (One-way ANOVA, p = 0.34) (Figure 1E, 1F). In addition to the global, widespread calcium transients, we also observed in individual spines, calcium signals that were not correlated with dendritic signals (Figure 1- figure supplement 1), indicating that we could resolve spine calcium signals in our experimental conditions.

We then assessed whether these widespread, highly correlated apical tuft calcium signals were modulated by visual stimulation and locomotion. We found that both visual stimulation and locomotion increased calcium signals in the apical tuft of layer 5 neurons (average ΔF/F0; repeated measures Two-way ANOVA, p = 0.005, 0.003 and 0.99 for visual stimulation, locomotion and interaction between both conditions, respectively; n = 14 neurons) (Figure 1H). However, the correlation of calcium signals between all imaged dendritic branches remained high (r ≥ 0.92) during periods of darkness and visual stimulation as well as during stationary and locomotion periods, without a significant difference across conditions (Two-way ANOVA, p = 0.43, 0.62 and 0.97 for visual stimulation, locomotion and interaction between both conditions, respectively).

124 In line with these findings, we found that branch-specific activity in the apical tuft was
125 rare. We quantified the amount of branch-specific activity in all pairs of branches belonging
126 to the same neuron as the proportion of calcium transients present in one branch and absent
127 in the other. Among the 70 imaged branches across 14 neurons, branch-specific calcium
128 transients represented less than 3% of the total number of transients. Among all imaged
129 calcium transients, these local signals were dominated by calcium transients of the smallest
130 amplitudes (Figure 1J). In addition, neither visual stimulation nor locomotion significantly
131 affected this small proportion of branch-specific calcium signals (Three-way ANOVA, $p < 10^{-15}$
132 for event amplitude and $p = 0.29$; 0.8 and 0.94, for visual stimulation, locomotion and
133 interaction between both conditions, respectively. No other interaction effect was
134 statistically significant) (Figure 1I). We tested the robustness of our quantification by using
135 different thresholds for the detection of individual calcium transients (Figure 1- figure
136 supplement 2A and 2B). We found that lowering the threshold by 30% in one of the two pair
137 branches reduced the proportion of branch-specific events from 3.8% to 0.8%, suggesting that
138 most of these already rare events were near detection threshold (Figure 1- figure supplement
139 2B). We also confirmed that our results were not affected by the time window that we used
140 to detect coincident events in pairs of dendritic branches (Figure 1- figure supplement 2D, 2E.
141 Altogether, our results show that apical dendritic calcium signals in V1 layer 5 neurons
142 are almost exclusively dominated by highly correlated calcium transients in the whole apical
143 tuft regardless of the dendritic branching order. Neither visual stimulation nor locomotion
144 modulated this high correlation between apical tuft dendritic calcium signals.
145

146 Calcium signals are highly correlated throughout all compartments of 147 individual layer 5 neurons

148 We then assessed how global, widespread apical tuft calcium signals were coupled across
149 neuronal compartments. For this, we semi-simultaneously imaged GCaMP6s calcium signals
150 at two focal planes, separated on average by 170 µm in depth, in 4 different pairs of neuronal
151 compartments from the soma to the apical tuft: Soma-Trunk, proximal Trunk-distal Trunk,
152 distal Trunk-apical Tuft, proximal Tuft-distal Tuft (Figure 2A, 2B). We used GCaMP6s which
153 has higher signal amplitude and signal-to-noise ratio than GCaMP6f, in order to maximise our
154 ability to detect somatic signals (Chen *et al.*, 2013). We found that calcium transients

155 simultaneously imaged in each pair of proximal and distal compartments were highly
156 correlated (Figure 2C, 2D). Since the rise and decay kinetics of calcium events were slower in
157 the soma than in the dendrites, we performed our quantification on individual peaks of
158 calcium transients (see Methods). For each pair of compartments, we found that the average
159 Pearson's correlation value between the peak amplitude of individual transients was 0.88
160 between the proximal and distal parts of the apical tuft, 0.92 between the trunk and the apical
161 tuft and 0.85 between the proximal and distal trunk (Figure 2D and Figure 2-figure
162 supplement 1). The lowest correlation value was found between the soma and the proximal
163 trunk (0.74, Figure 2D). These results also confirmed the high correlation of calcium transients
164 throughout the apical tuft (Figure 2A, 2D(i)), that we found in our single-plane imaging
165 experiments (Figure 1D, 1F). We checked whether the small proportion of events (3%)
166 detected as branch-specific in apical tuft dendrites were also found in the apical trunk. On
167 average, we found that 60% of the events detected as branch-specific were also found in the
168 trunk (Figure 2-figure supplement 2).
169 Altogether, these results show that calcium transient amplitudes were highly
170 correlated from the soma to the distal apical tuft of V1 layer 5 neurons.
171

172 Frequency of calcium transients decreases in a distance- and amplitude 173 dependent manner from soma to apical tuft

174 We then tested whether the high correlation of calcium transient amplitudes from the soma
175 to the apical tuft was associated with distance-dependent changes in the frequency of these
176 events. We quantified the frequency of calcium events in each pair of proximal and distal
177 compartments imaged semi-simultaneously (Figure 3A). We found that the frequency of
178 calcium transients decreased from proximal to distal compartments (Paired t-test, $p = 1.1e^{-6}$,
179 n = 31 pairs of compartments from 19 neurons) by an average of 14% from soma to proximal
180 trunk, 8% from proximal to distal trunk, 24% from distal trunk to apical tuft and 22% from
181 proximal tuft to distal tuft (Figure 3B). From these proportions, we estimated a decrease of
182 about 40% of calcium transients from soma to the distal part of the apical tuft (Figure 3- figure
183 supplement 1A, 1B). This result was confirmed by a second data set, in which somatic and
184 apical tuft calcium transients were imaged independently (at 120 Hz) in individual layer 5
185 neurons. We found that the mean frequency of calcium transients in the apical tuft

corresponded to 62% of the frequency of events in the corresponding soma (n= 13 neurons Figure 3-figure supplement 1).

We then checked whether this decrease in frequency depended on the amplitude of the calcium transients. We calculated the percentage of compartment-specific calcium transients as a function of their amplitude (Figure 3C). Our results show that smaller amplitude calcium transients in the proximal compartment were more likely to attenuate below detection level in the distal compartment compared to larger amplitudes events (red trace in figure 3C). The vast majority of compartment-specific events were dominated by calcium transients in proximal compartments that were not detected in distal ones (red trace in figure 3C), while only few calcium transients were found in distal compartments and not in the corresponding proximal compartment (blue trace in Figure 3C) (see also Supplementary video 1 and 2). As a result, compartment-specific events were dominated by small amplitude calcium transients that attenuated from proximal to distal compartments (Two-way ANOVA, $p<10^{-15}$, $p<10^{-15}$, $p<10^{-15}$, for compartment (proximal vs distal), amplitude, and interaction effect, respectively; Figure 5A). Our results were robust to the threshold (+/- 30%) that was used for detecting calcium transients (Figure 1-figure supplement 2A, 2C). Our results were also robust to the time window that was used to detect simultaneous events in different compartments (Figure 1-figure supplement 2D, 2F). Notably, we also observed relatively large calcium transients in soma and proximal trunk that were not detected in the distal compartment (see examples in figure 3B(iii) and 3B(iv) and percentage of compartment-specific event in Figure 3C(iii) and 3C(iv) for $\Delta F/F0>0.3$), suggesting the presence of active mechanisms inhibiting calcium transients along the apical trunk.

These results indicate that almost all distal events were found in proximal compartments and that at least 40% of somatic calcium transients attenuate in a distance-dependent manner along the apical trunk and distal dendrites. Thus, somato-dendritic coupling in layer 5 neurons is strong, but asymmetric.

Ex vivo calibration of GCaMP6s and GCaMP6f signals in layer 5 soma and apical tuft dendrites

We next sought to characterize the electrophysiological activity underlying our observations of strong, but asymmetric, somato-dendritic coupling *in vivo*. We reasoned that neuronal

217 spiking driven by stimulation of the soma and apical tuft would differentially impact calcium
218 event amplitudes in proximal and distal neuronal compartments. We examined this *ex vivo*
219 by combining calcium imaging and whole-cell recordings in acute cortical slices from mouse
220 V1. We imaged the soma and distal apical dendrite (nexus) of GCaMP6s- and GCaMP6f-
221 expressing layer 5 neurons whilst driving neuronal spiking either by somatic current injections
222 (somatic stimulation) or L1 electrical stimulation (dendritic stimulation) (Figure 4A). Somatic
223 and dendritic stimulation consisted of a train of 10 suprathreshold stimuli delivered at 5-
224 200Hz; each stimulus reliably triggered single action potentials (Figure 4B). Action potentials
225 evoked by dendritic stimulation were accompanied by an enhanced afterdepolarization in the
226 soma, characteristic of distal dendritic electrogenesis (Larkum, Kaiser and Sakmann, 1999;
227 Shai *et al.*, 2015).

228 For somatic stimulation, we found that we could robustly detect somatic calcium
229 signals with firing frequencies as low as 5 Hz with GCaMP6s (Figure 4E, 4G), and as low as 25
230 Hz with GCaMP6f (Figure 4F, 4H); we could not reliably detect calcium events associated with
231 single action potentials with either indicator ($\Delta F/F0$ peak for GCaMP6s: mean = 0.02, sem =
232 0.01, t-test vs null, $p = 0.07$, n = 10 neurons; $\Delta F/F0$ peak for GCaMP6f: mean = -0.02, sem =
233 0.03, t-test vs null, $p = 0.39$, n = 9 neurons). Somatic signal amplitude increased monotonically
234 with stimulation frequency for both indicators, with a plateau at 100-200 Hz. By contrast, in
235 the distal dendrites, reliable signals for both indicators were only detected when somatically-
236 driven spiking exceeded 50Hz (Figure 4E-4H), likely reflecting the critical frequency (50-100Hz)
237 of back-propagating action potentials required to trigger distal dendritic calcium spikes
238 (Larkum, Kaiser and Sakmann, 1999; Shai *et al.*, 2015). For dendritic stimulation, calcium
239 signals were reliably detected in both the soma and distal dendrites. With GCaMP6s, this was
240 true for all frequencies tested (Figure 4C, 4E, 4G). With GCaMP6f, somatic signals could not
241 be observed at lower stimulation frequencies (5 Hz) (Figure 4D, 4F, 4H).

242 Our findings suggest that: 1) somatically-triggered back-propagating action potentials
243 below the critical frequency (<50-100Hz) may underlie the distant-dependent loss of dendritic
244 calcium signals we observed *in vivo*; 2) spiking driven by strong apical tuft input or high-
245 frequency spiking driven by somatic depolarization may underlie the strong somatic-dendritic
246 coupling detected *in vivo*.

247 Notably, compared to GCaMP6s, GCaMP6f had a reduced sensitivity for detecting
248 calcium signals, specifically in the soma during low frequency spiking driven either by somatic

249 or dendritic stimulation (Figure 4E-4H). Consequently, as compared to GCaMP6s, attenuation
250 of events from soma to dendrite was underestimated whereas attenuation of events from
251 dendrite to soma was overestimated with GCaMP6f (Figure 4G vs 4H). With GCaMP6s, by
252 contrast, attenuation of signals was asymmetric; we only found attenuation from soma to
253 distal dendrites, as observed *in vivo* (Figure 4G).
254

255 Visual stimulation and locomotion do not alter the coupling of calcium signals 256 between neuronal compartments from soma to apical tuft

257 We then tested whether visual stimulation and locomotion altered the coupling between the
258 different compartments of individual layer 5 neurons. For each condition, we plotted the
259 percentage of compartment-specific calcium transients as a function of their amplitude. We
260 found that in all four conditions compartment-specific events were dominated by small
261 amplitude calcium transients in proximal compartments: there was no significant difference
262 between darkness and visual stimulation periods, both during stationary and locomotion
263 periods (Figure 5B; Three-way ANOVA, $p = 0.69$, $p = 0.21$ and $p = 0.64$ for visual stimulation,
264 locomotion, and interaction respectively; $p < 10^{-15}$ for event amplitude; no other interaction
265 was found to be statistically significant). Similarly, we found no significant difference between
266 behavioural states defined by stationary, locomotion and transition periods from still to
267 running activity (see methods), either during visual stimulation or in darkness (Figure 5-figure
268 supplement 1A). These results indicate that the function relating calcium transient amplitude
269 and percentage of attenuated events from soma to apical tuft remained unchanged by visual
270 stimulation and behavioural-state changes. In addition, we found that, on average, the
271 percentage of coincident calcium signals across compartments of individual neurons was not
272 significantly modified either by visual stimulation or behavioural state changes (n=19
273 neurons) (Figure 5-figure supplement 1B and Figure 5-figure supplement 2).
274 Even though smaller events were attenuated with similar probabilities across the four
275 conditions, calcium transients that do propagate through different neuronal compartments,
276 may be amplified or attenuated in a condition-dependent manner (Figure 5C). To capture
277 these nonlinearities, we plotted the amplitude of each detected transient in each
278 compartment and calculated a residual value as the distance from the linear robust regression
279 fit (Figure 5C). We then plotted the cumulative distribution of the residual value for every

280 calcium transient in all 4 pairs of imaged compartments from soma to apical tuft (Figure 5D).
281 We found that, on average, the non-linear changes in calcium transient amplitude across
282 neuronal compartments were neither significantly affected by locomotion nor by visual
283 stimulation (Three-way ANOVA, p = 0.96, p = 0.23 and p = 0.91 for visual stimulation,
284 locomotion and interaction effect, respectively; p = 0.86 for different compartments; no other
285 interaction effect was found to be significant; n = 11 Soma–Trunk pairs; n = 5 pTrunk–dTrunk;
286 n = 9 Trunk–Tuft; n = 6 pTuft-dTuft from 19 neurons). These results indicate that, while
287 locomotion and visual stimulation increase the activity of layer 5 pyramidal neurons, the
288 relationship between the amplitude of calcium transients and the probability of coupled
289 events across compartments remains unchanged. Independently of each condition, single
290 calcium transients of a given amplitude have the same probability of being compartment-
291 specific.

292 Since layer 5 neurons in V1 respond selectively to drifting grating orientations and that
293 dendritic spikes triggered by visual input were suggested to enhance somatic tuning to the
294 preferred orientation (Smith *et al.*, 2013), we quantified the impact of grating orientation on
295 the correlation of calcium transients throughout neuronal compartments. In the apical tuft,
296 we found that the selectivity of the responses to the drifting gratings orientation, quantified
297 by an orientation selectivity index (OSI), did not affect the high correlation of calcium
298 transients between tuft dendrites (Figure 6A-D). We then compared orientation selective
299 responses during stationary and locomotion periods both in apical tufts and corresponding
300 somata (n=15 neurons) (Figure 6E, 6F). We found that locomotion similarly increased calcium
301 transient amplitudes both in apical tuft and soma, without a significant difference between
302 compartments (Figure 6G, Paired t-test, p = 0.38), both during the presentation of preferred
303 and non-preferred orientations (Figure 6H, Repeated measures Two-way ANOVA on log-
304 transformed data, p = 0.07, 0.71 and 0.28 for stimulus-type, compartment and interaction
305 effects respectively). As a consequence, the OSI of somatic and apical tuft responses remained
306 unchanged during both stationary and locomotion periods (Figure 6I, Repeated measures
307 Two-way ANOVA, p = 0.49, p = 0.42 and p = 0.45, for the effects of locomotion, neuronal
308 compartment and interaction, respectively). In line with these results, we found that the
309 preferred orientation was similar throughout tuft dendritic branches and neuronal
310 compartments of individual neurons, both during stationary and locomotion periods (Figure
311 6J and K). Finally, the Pearson's correlation between apical tuft branches calcium signals and

312 across neuronal compartments remained high and unchanged regardless of the gratings
313 orientation (Figure 6L, 6M).
314 Altogether, these results indicate that calcium signals in individual layer 5 pyramidal
315 neurons are highly correlated throughout apical tuft branches and neuronal compartments,
316 and that this high somato-dendritic coupling remains unchanged by visual stimulation and
317 locomotion.
318

319 ## Discussion

320 Our results show that GCamP6f and GCamP6s calcium transients are highly correlated in
321 apical tuft dendrites of individual layer 5 neurons in the primary visual cortex of awake
322 behaving mice; branch-specific calcium transients were rare and limited to small amplitude
323 transients. GCaMP6s calcium transients were also found to be highly correlated throughout
324 all compartments of individual neurons (soma, trunk, tuft). However, their frequency was
325 found to decrease in a distance-dependent manner from soma to apical tuft. Whereas almost
326 all transients observed in the tuft were present in proximal compartments, the frequency of
327 calcium transients in apical tuft was about 60% of their frequency in the corresponding soma.
328 *Ex vivo* experiments suggest that attenuated dendritic signals were likely associated with low
329 frequency back-propagating action potentials, whereas highly correlated somato-dendritic
330 signals were likely associated with high frequency somatic activity, or strong apical tuft inputs.
331 Neither visual stimulation nor locomotion altered either the coupling between neuronal
332 compartments from soma to apical tuft, nor the proportion of tuft branch-specific events.
333

334 ## Limitations of the use of calcium imaging to assess dendritic activity in awake
335 behaving mice

336 Investigations of local dendritic activity in awake behaving mice have so far mainly relied on
337 the use of genetically-encoded calcium indicators (Xu *et al.*, 2012; Cichon and Gan, 2015;
338 Manita *et al.*, 2015; Takahashi *et al.*, 2016; Sheffield, Adoff and Dombeck, 2017; Kerlin *et al.*,
339 2018; Ranganathan *et al.*, 2018; Sheffield and Dombeck, 2019). The analysis of our data set
340 showed that several experimental constraints may bias results towards signals mistakenly
341 interpreted as local dendritic activity. Dense labelling was already demonstrated to strongly
342 affect correlation values (Xu *et al.*, 2012); even in cases of relatively sparse labelling of

individual neurons, contamination from axons or dendrites of other labelled neurons may lead to local signals detected in single dendrites. In our data set, we systematically reconstructed our imaged neurons and excluded regions of interest where overlapping dendrites from other neurons were observed. Movement artefacts may also lead to inaccurate detection of local dendrite signals; these artefacts are more likely to be found during specific behaviour, such as locomotion, and therefore can bias the interpretation of the results. In our data set we used the activity-independent marker tdTomato to correct for motion artefacts and excluded the recordings in which tdTomato marker was not detected. For most of our imaged neurons, baseline fluorescence of both GCaMP6s and GCaMP6f could also be used for the same purpose. Another parameter that may cause artefactual local dendritic signals, is the length of the imaged dendritic segments (and therefore the size of the regions of interest used to extract the changes of fluorescence over time). Small regions of interest could include spines not clearly distinguishable from the corresponding dendritic shaft, especially when the spine is located above the dendrite at the imaged focal plane. As a consequence, in small regions of interests, spine signals may be incorrectly interpreted as local dendritic signals.

Differences in calcium buffering properties of individual compartments also create detection biases as they lead to different decay times of fluorescent calcium indicators between somatic and dendritic compartments (Kerlin *et al.*, 2018; Beaulieu-Laroche *et al.*, 2019). In order to account for this difference, we based our analysis on the detection of peak amplitudes of individual calcium transients. This detection depends on arbitrary thresholds: we thus showed the robustness of our results across different detection thresholds (Figure 1-figure supplement 2). An additional source of bias is linked to the affinities of calcium indicators. Previous studies have shown that dendritic calcium spikes can reliably be detected with calcium indicators of lower sensitivity than GCaMP6f and GCaMP6s (Helmchen *et al.*, 1999; Xu *et al.*, 2012). However, while it was shown that GCaMP6 could detect individual somatic action potentials in layer 2/3 neurons *in vivo* (Chen *et al.*, 2013), this is not the case for GCaMP6f in layer 5 neurons (Beaulieu-Laroche *et al.*, 2019), nor for GCaMP6s based on our own *ex vivo* experiments. We did however find that GCaMP6s was superior in detecting somatic calcium events during low frequency spiking (<25 Hz) (Figure 4). Nonetheless, the detection of somatic action potentials in layer 5 neurons *in vivo* with GCaMP sensors may be

374 biased towards larger events, and as a consequence, the attenuation from soma to tuft may
375 be underestimated.
376

377 Widespread, correlated calcium transients in apical tuft dendritic branches of 378 layer 5 neurons

379 Our results show that in the apical tuft, calcium transients were highly correlated regardless
380 of how distal the imaged branches were from the nexus. Branch-specific calcium
381 transients were rare and limited to transients of the smallest amplitudes. These findings
382 suggest that either branch-specific calcium activity is virtually absent or that branch-specific
383 activity is systematically coincident with global tuft calcium events and thus could not be
384 detected with the temporal resolution of GCaMP6f or GCaMP6s. In addition, these results
385 indicate that active dendritic integration in the apical tuft is widely recruited across different
386 behavioural and sensory conditions. This widespread calcium activity throughout the layer 5
387 apical tuft may strongly influence plasticity and learning (Magee and Johnston, 1997; Golding,
388 Staff and Spruston, 2002; Kampa, Letzkus and Stuart, 2006; Sjöström and Häusser, 2006;
389 Remy and Spruston, 2007; Bittner *et al.*, 2017; Bono and Clopath, 2017; Guerguiev, Lillicrap
390 and Richards, 2017).
391

392 High but asymmetric coupling of calcium signals from soma to apical tuft

393 Our results show an asymmetry in the coupling between somatic and apical dendritic calcium
394 signals. Previous studies have shown that dendritic signals attenuate in a distance-dependent
395 manner, suggesting that at least some of the calcium events generated in one compartment
396 would fully attenuate as they reach the next compartment (Stuart, Schiller and Sakmann,
397 1997; Svoboda *et al.*, 1997; Helmchen *et al.*, 1999; Vetter, Roth and Häusser, 2001; Larkum *et*
398 *al.*, 2009). To estimate the lower bound proportion of calcium events generated in the tuft
399 and in the soma, we investigated the proportion of attenuated events in both somatofugal
400 and somatopetal directions. Our results show that while around 40% of somatic calcium
401 transients decay by the time they reach the apical tuft, only 1.4% of apical tuft calcium events
402 were not associated with somatic events (Figure 5A). These results indicate that at least 40%
403 of somatic calcium transients were not triggered by apical tuft calcium events, and that these
404 transients attenuated from the soma to the apical tuft. Based on our *ex vivo* recordings, we

405 suggest that attenuated calcium transients are associated with low-frequency back-
406 propagating somatic action potentials, below the critical frequency required to trigger
407 dendritic electrogenesis (Larkum, Kaiser and Sakmann, 1999; Shai *et al.*, 2015). Attenuation
408 may also involve active inhibitory mechanisms along the somato-dendritic axis (Larkum,
409 Kaiser and Sakmann, 1999; Naka and Adesnik, 2016).

410 A recent study reported a high and symmetric somato-dendritic coupling in V1 layer 5
411 neurons concluding that GCaMP6f events occurred concurrently in soma and dendritic
412 compartments (Beaulieu-Laroche *et al.*, 2019). The authors reported that 83.9 % (median) of
413 dendritic calcium signal (rise events) were paired with events in the soma while 73.4% of
414 somatic events were paired with dendritic ones. This discrepancy may be explained by
415 differences in imaging conditions including a denser labelling, which increases the amount of
416 background signals, and the use of GCaMP6f, which has a lower signal amplitude and signal-
417 to-noise ratio than the GCaMP6s indicator used in our study, leading to a lower probability of
418 detecting small events in layer 5 somata, as shown by our *ex vivo* recordings (Figure 4G).

419 In our study, we estimated that 60% of somatic calcium signals were highly correlated
420 with global apical tuft calcium signals. Based on our *ex vivo* experiments, high somato-
421 dendritic coupling would occur during either 1) high frequency back propagating action
422 potentials or 2) strong apical tuft activity capable of driving somatic spiking. Coupling could in
423 principle also be observed with lower frequency back propagating action potentials, provided
424 they are paired with tuft inputs (Larkum, 2013; Manita *et al.*, 2015). Further experiments are
425 needed to resolve these potential mechanisms *in vivo*, for example using voltage-sensitive
426 dyes (Chavarha *et al.*, 2018; Roome and Kuhn, 2018; Adam *et al.*, 2019) or dendritic
427 electrophysiological recordings (Moore *et al.*, 2017), that would provide the temporal
428 resolution to resolve the different types of dendritic events.

429 Notably, both apical tuft signals and the somato-dendritic coupling may differ
430 between different subtypes of layer 5 pyramidal neurons. It is known that at least two main
431 types exist: intratelencephalic neurons which connect cortical areas, and pyramidal tract
432 neurons which project to multiple subcortical areas (Harris and Shepherd, 2015; Gerfen,
433 Economo and Chandrashekar, 2018). These two types display different morphologies (Groh
434 *et al.*, 2010) and receive different types of inputs (Young *et al.*, 2019). The neurons included
435 in this study had their soma located at various depths within layer 5 (median 528 μm, see
436 Figure 3-Figure Supplement 1) and mainly displayed thick-tufted morphology, characteristic

437 of pyramidal tract neurons. Since we selected the imaged neurons visually based on their
438 GCaMP6 fluorescent signal, our sampled is likely biased towards layer 5 neurons with thick
439 trunk and thick-tufted morphology.
440

441 Integration of visual and locomotion-related inputs in layer 5 neurons in awake 442 behaving mice

443 Our results show that, in our passive viewing conditions, changes in visual inputs (darkness
444 versus drifting gratings) and locomotion-related inputs do not affect the relationship between
445 somatic, trunk and apical tuft calcium signals nor the prevalence of branch-specific dendritic
446 events in the apical tuft. These results are in agreement with a previous study showing that
447 somato-dendritic correlations of calcium transients remain unchanged by visual stimulation
448 and locomotion (Beaulieu-Laroche *et al.*, 2019). It is however possible that in both studies,
449 untracked behavioural states (e.g. arousal, attention) during stationary and locomotion
450 periods may differentially shape somato-dendritic activity.

451 It is known that the prevalence and the dynamics of synaptic inputs received by layer
452 5 pyramidal neurons strongly vary between passive sensory stimulation and active learning
453 tasks (Xu *et al.*, 2012; Hong *et al.*, 2018). Apical tuft dendrites of layer 5 neurons receive a
454 barrage of thousands of synaptic inputs *in vivo* (Stuart and Spruston, 2015) and it was shown
455 that V1 neurons receive synaptic inputs conveying information not only about visual stimuli
456 but also about internal variables (arousal/attention, motor activity, spatial information)
457 (Pakan *et al.*, 2016, 2018; Pakan, Francioni and Rochefort, 2018). Finally, in addition to
458 excitatory inputs, both inhibitory and neuromodulatory inputs were shown to modulate
459 electrical interactions between soma and dendrites in layer 5 neurons (Larkum, Kaiser and
460 Sakmann, 1999; Silberberg and Markram, 2007; Labarrera *et al.*, 2018; Williams and Fletcher,
461 2019).

462 It is therefore possible that during the active learning of a behavioural task, the
463 synaptic inputs associated with this learning process would lead to different mechanisms of
464 dendritic integration than during passive viewing. For example, dendritic integration of
465 multiplicative combinations of sensory and motor inputs in the tuft dendrites of layer 5
466 pyramidal neurons has been described during an active sensing task in mouse somatosensory
467 cortex (Ranganathan *et al.*, 2018). In addition, it was proposed that changes in neuronal

468 representations during learning would rely on active dendritic signals generating calcium
469 plateau potentials (Bittner *et al.*, 2015; Grienberger *et al.*, 2017). In that case, somato-
470 dendritic coupling may change during the course of learning (Sheffield, Adoff and Dombeck,
471 2017). This remains to be tested in the visual cortex. Similarly, somato-dendritic coupling may
472 evolve during postnatal development when sensori-motor associations are formed. Recently,
473 it was shown in the mouse primary visual cortex, that dendrites of layer 2/3 neurons increase
474 their coupling during adulthood, as a consequence of decreased responsiveness of dendrite-
475 targeting interneurons to locomotion-related inputs (Yaeger, Ringach and Trachtenberg,
476 2019). Further investigations are needed to reveal these mechanisms in layer 5 visual cortical
477 neurons.

478 **Materials and Methods**

479 **Animals**

480 All experiments and procedures involving animals were approved by the University of
481 Edinburgh Animal Welfare and the ethical review board (AWERB). Experiments were
482 performed under the appropriate personal and project licenses from the UK Home Office in
483 accordance with the Animal (Scientific Procedures) act 1986 and the European Directive
484 86/609/EEC on the protection of animals used for experimental purposes. Adult male and
485 female mice, aged between 8 to 10 weeks, were obtained from Jackson Laboratory, ME, USA
486 (B6.Cg-Gt(ROSA)26Sor$^{tm14(CAG\text{-}tdTomato)Hze}$/J [RRID:IMSR_JAX:007914]). Mice were group caged
487 in groups of 2-6 animals, with a running wheel and on a reverse 12:12 hour light/dark cycle,
488 with ad libitum access to food and water.

489 **Surgical procedures**

490 Viral delivery of GCaMP6

491 To obtain sparse labelling of excitatory neurons we used a Cre-dependent approach, by co-
492 injecting viral constructs AAV1.CamKII 0.4.Cre.SV40 (Penn Vector core catalogue No. 105558-
493 AAV1) diluted at 1:10000 or 1:20000 with either AAV1.Syn.Flex.GCaMP6f.WPRE.SV40 (Penn
494 Vector Core, catalogue No. 100833-AAV1) or AAV1.Syn.Flex.GCaMP6s.WPRE.SV40 (Penn
495 Vector Core, catalogue No. 100845-AAV1) diluted 1:10 in the final solution. All dilutions were

496 made in sterile artificial cerebrospinal fluid (ACSF). AAV1.Syn.Flex.GCaMP6f.WPRE.SV40 was
497 used for single plane imaging of the apical tuft while AAV1.Syn.Flex.GCaMP6s.WPRE.SV40 was
498 used for semi-simultaneous two-planes imaging. Animals were initially anesthetized with 4%
499 Isoflurane and subsequently maintained on 1-2% isoflurane throughout the procedure. Body
500 temperature was maintained at physiological levels using a closed-loop heating pad. Eye
501 cream (Bepanthen, Bayer) was applied to protect the eyes from dryness and light exposure.
502 After induction of anaesthesia, mice were shaved, mounted onto a stereotaxic frame
503 (David Kopf instruments, CA, USA) and head-fixed using ear bars. An analgesic was
504 administered subcutaneously (Vetergesic, buprenorphine, 0.1 mg/kg of body weight). Viral
505 injections were performed in the primary visual cortex of left hemispheres (centred around
506 2.5 mm lateral from midline and 0.5 mm anterior to lambda) at 650 and 500 µm from brain
507 surface using a glass pipette (20 µm tip diameter, Nanoject, Drummond Scientific), coupled
508 to a Nanoject II (Drummond Scientific). A total volume of 55.2 nl was injected across the two
509 depths (6 x 4.6 nl at each location with 30s intervals between each injection to allow sufficient
510 time for diffusion). After each injection, pipettes were left in situ for an additional 5 minutes
511 to prevent backflow. The scalp was then sutured (Ethicon, Ethilon polyamide size 6) and the
512 animal monitored during recovery in a heated cage before returning to its home cage for 2-3
513 weeks.

514 Headplate and imaging window

515 Under anaesthesia (isoflurane), mice were shaved, mounted onto a stereotaxic frame (David
516 Kopf instruments, CA, USA) and head-fixed using ear bars. Analgesic and anti-inflammatory
517 drugs were administered subcutaneously (Vetergesic, buprenorphine, 0.1 mg/kg of body
518 weight; Carpaphen, Carprieve, 5mg/kg of body weight; Dexamethasone, Rapidexon, 2mg/kg
519 of body weight). For a cranial window over V1, a section of scalp was removed, the underlying
520 bone was cleaned before a rectangular craniotomy of about 2x1.5 mm was made over the
521 left primary visual cortex (centred around 2.5 mm lateral and 0.5 mm anterior to lambda).
522 The dura was kept intact. The craniotomy was then sealed with a glass cover slip and fixed
523 with cyanoacrylate glue. To stabilize the brain during imaging, we used a triple glass window
524 by stacking three cover-slip glasses (Menzel-Glaser 24x32 mm # 0) on top of each other. These
525 were glued together using an optically clear UV-cured glue (Norland Optical adhesive).
526 Overall, the thickness of the glass window inserted through the cranial window, was

527 comparable to the thickness of the skull at the time of imaging. A custom-built metal
528 headplate was fixed on top of the skull with glue and cemented with dental acrylic (Paladur,
529 Heraeus Kulzer). At the end of the procedure, a single dose of 25mL/kg of Ringer's solution
530 was injected subcutaneously to rehydrate the animal after the procedure. The animal was
531 then released from the head fixation and returned to a heated recovery cage, until full motor
532 capacity was recovered.

533 *In vivo* two-photon imaging data acquisition

534 Imaging was performed using a 25x Objective (Olympus). The excitation wavelength of the
535 laser was set to 920 nm. Layer 5 pyramidal neurons were recorded between 500 and 650 µm
536 below the brain surface and followed up to their distal tuft dendrites along the apical trunk.
537 Neurons which had their nucleus filled with GCaMP6 or had blebbed dendrites were excluded
538 for recording. At the end of each imaging session, a z-stack was acquired to allow a more
539 detailed, offline morphological reconstruction of the imaged neuron. Reconstructions were
540 done using the ImageJ plugin Simple Neurite Tracer. Imaging was performed using a 570 nm
541 short-pass dichroic mirror and two single-band pass filters, a 525/50 (Scientifica) for GCaMP6
542 light absorption, and a 620/60 (Scientifica) for TdTomato absorption.

543 Habituation and imaging started 2–3 weeks after AAV injection. Mice were habituated
544 to head-fixation in the dark for 45 min and began to run freely on a polystyrene cylindrical
545 treadmill (20 cm diameter, on a ball-bearing mounted axis). Running speed on the treadmill
546 was continuously monitored using an optical encoder (E7P, 250cpr, Pewatron, Switzerland)
547 that was connected to a data acquisition device (National Instrument, UK). Data was recorded
548 with custom-written software in LabView (National Instrument, UK) and analysed in MATLAB
549 (Mathworks, MA).

550 Single-plane two-photon imaging data were acquired using a custom-built galvo-
551 resonant scanning system with a Ti:Sapphire pulsing laser (Chameleon Vision-S, Coherent, CA,
552 USA; < 70 fs pulse width, 80 MHz repetition rate) at 120 Hz, with a custom-programmed
553 LabVIEW-based software (version 8.2; National Instruments, UK). Multi-plane data were
554 acquired using an ultra-fast, solid-state, single 100 fs pulse width laser (InSight DeepSee,
555 SpectraPhysiscs, CA, USA) and a FemtoSmart Dual two-photon microscope (Femtonics,
556 Budapest, Hungary). Two focal planes (512x165 pixels), with an average distance of 170 µm
557 in Z, were imaged at a frequency of 96 frames/s (48 frames/s per plane) using a Piezo

558 objective positioner kit (P725.4CA, Physic Instruments, Germany), switching between planes
559 at 9.6 Hz (4.8 Hz per plane).

560 Visual stimulation

561 Visual stimuli were generated using the Psychophysics Toolbox package (Brainard, 1997) for
562 MATLAB (Mathworks, MA) and displayed on a custom-modified, backlit LED monitor (51 × 29
563 cm, Dell, UK), which wasplaced 20 cm from the right eye, covering 104° × 72° of the visual
564 field. Visual stimulation trials consisted of drifting full-field square-wave gratings for
565 3 seconds (spatial frequency of 0.05 cycles per degree, 1.5 Hz, 8 equally spaced directions in
566 randomized order, contrast 80%, mean luminance 37 cd/m^2). Drifting grating presentations
567 were separated by 4 second periods of isoluminant grey stimuli. We acquired 8-12 trials in
568 darkness and 12-20 trials during visual stimulation for each imaged field of view. Time stamps
569 for the onset of every stimulus were recorded and aligned to imaging frames using custom-
570 built Matlab scripts.

571 ***In vivo* data Analysis**

572 Image analysis and signal extraction

573 To correct for brain motion after image acquisition, we used 2D plane translation-based image
574 alignment (SIMA 1.2.0, sequential image analysis; Kaifosh et al., 2014). We 3D reconstructed
575 each imaged neuron and defined regions of interest (ROIs) corresponding to neuronal cell
576 body and dendritic segments manually. Due to sparse labelling, signal contamination was
577 negligible in most cases. ROIs that were contaminated by labelled structures from other
578 neurons were excluded from further analysis.

579 The pixel intensity within each ROI was averaged to create a raw fluorescence time
580 series F(t). Baseline fluorescence F0 was computed for each neuron by taking the fifth
581 percentile of the smoothed F(t) (1 Hz lowpass, zero-phase, 60th-order FIR filter) over each
582 trial (F0(t)), averaged across all trials. As a consequence, the same baseline F0 was used for
583 computing the changes in fluorescence in darkness and during visual stimulation. The change
584 in fluorescence relative to baseline, ΔF/F0 was computed by taking the difference between F
585 and F0(t) and dividing by F0.

586 Single plane data was acquired at 120 Hz, and subsequently downsampled to 5Hz for
587 signal processing. Multi-plane data were analysed at 4.8 Hz.

588 ## Calcium transient analysis

589 We first estimated noise levels by filtering our ΔF/F0 signal using a 9th order, zero-phase, high-
590 pass filter at 0.6 Hz (Matlab function *filter*). We then estimated the standard deviation of the
591 filtered signal and used a threshold of 2.8 of this standard deviation to detect individual
592 calcium transients, using the built-in Matlab function *findpeaks.* We tested the robustness of
593 our results to different thresholds +/- 30% of the selected threshold (Figure 1-figure
594 supplement 2).

595 For each peak found in any branch or compartment, we defined a calcium transient as
596 coincident in another branch or compartment when it occurred in a time window of 3 seconds
597 around the frame where the first peak was originally detected (2 seconds before, 1 after). As
598 a consequence, peaks detected as coincident could not be further apart than 2 seconds.
599 Figure 1-figure supplement 2 shows the distribution of time intervals between events
600 detected as coincident. The mean time interval was close to 0 (2.19xe^{-4} seconds) with
601 standard deviation of 0.28 seconds, meaning that 95% of all coincident events were found
602 within a time interval of 0.56 seconds. Each calcium transient could only be considered
603 coincident with one transient. The peak amplitude of a calcium transient was determined by
604 taking the difference between the ΔF/F0 amplitude at the frame in which the peak was
605 detected and a local minimum in a 2 seconds, backward sliding window. Correlation values
606 were calculated as the Pearson's correlation values between peak calcium transient
607 amplitudes in pairs of branches or compartments. Whenever a peak was detected in only one
608 compartment and not in the other (compartment-specific events), the correlation was made
609 between the peak amplitude in one compartment and the difference between the maximum
610 and minimum ΔF/F0 values in a 3 second window centred around the frame of the detected
611 peak in the other compartment. Shuffling values were obtained by randomly shuffling the
612 order of the events in one branch or compartment of each pair. Residuals were extracted by
613 calculating the robust linear regression line between normalised event amplitudes in two
614 compartments, and then extracting the distance, along the y-axis, of each individual point
615 from this robust line.

616 ## Locomotion analysis

617 Changes in the position of the cylindrical treadmill (sampled at 12,000 Hz) were interpolated
618 to match the rate of imaging. To define stationary and locomotion periods we used the
619 following criteria: Stationary corresponded to periods where the instantaneous speed (as
620 measured at the 40 Hz sampling rate) was less than 0.1 cm/s. Locomotion corresponded to
621 periods meeting three criteria: instantaneous speed ≥ 0.1 cm/s, 0.25 Hz lowpass filtered
622 speed ≥ 0.1 cm/s, and an average speed ≥ 0.1 cm/s over a 2 s window centered at this point
623 in time (Pakan *et al.*, 2016). Any inter-locomotion interval shorter than 500 ms was also
624 labelled as locomotion. Stationary periods less than 3 s after or 0.2 s before a period of
625 locomotion were removed from the analysis. For figure 5-figure supplement 1, behavioural
626 transitions were defined as time windows including: (1) 2 seconds before the onset of
627 locomotion as defined above and 1 second after the onset, as well as (2) 1 second before the
628 offset of locomotion and 20 seconds after the offset (unless another locomotion period began
629 before the 20 seconds) (Vinck *et al.*, 2015). For this analysis, behavioural transitions were
630 excluded from stationary and locomotion periods.

631 ## Orientation Selectivity

632 To determine the specific stimulus response parameters of each neuron to the oriented
633 gratings, the ΔF/F0 during each presented oriented stimulus was first averaged across all
634 trials. The preferred orientation of each neuron was the orientation that elicited the maximal
635 response when averaged across all trials. The orientation selectivity index (OSI) was calculated
636 as $(O_{pref}-O_{orth})/(O_{pref}+O_{orth})$ where O_{pref} represents the mean ΔF/F0 value during the
637 presentation of the preferred orientation across trials and O_{orth} represents the mean ΔF/F0
638 value during the presentation of the orientation orthogonal to the preferred one. For the
639 detailed analysis of orientation preference in Figure 6J and 6K, the preferred response angle
640 was estimated by calculating the argument of the resultant vector (V) in the complex plane,
641 which was given by:

642 $$V = \frac{\sum_k R(\theta_k) e^{2i\theta_k}}{\sum_k R(\theta_k)}$$

643 where $R(\theta_k)$ is the mean ΔF/F0 response to angle θ_k (Mazurek, Kager and Van Hooser, 2014).

644 ## ***Ex vivo*** **patch-clamp recordings and calcium imaging**

645 C57BL/6 mice (8-10 week old) were injected with either flexed GCaMP6s
646 (AAV1.Syn.Flex.GCaMP6s.WPRE.SV40; dilution 1:10; Penn Vector Core, catalogue 384 No.
647 100845-AAV1) or flexed GCaMP6f (AAV1.Syn.Flex.GCaMP6f.WPRE.SV40; dilution 1:10; Penn
648 Vector Core, 383 catalogue No. 100833-AAV1) along with CaMKII-Cre (AAV1.CamKII
649 0.4.Cre.SV40; diluted 1:100 or 1:1000; Penn Vector core catalogue No. 105558-AAV1)
650 targeted to Layer 5 in V1 (see Viral Delivery of GCaMP6 in Methods for details on the injection
651 parameters). 3-4 weeks following injection, animals were decapitated under isoflurane
652 anaesthesia. The brain was extracted and coronally sliced into 400 µm thick sections in ice
653 cold, carbogenated (95% O_2, 5% CO_2) dissection media (in mM: 87 NaCl, 75 sucrose, 2.5 KCl,
654 25 NaHCO3, 1.25 NaH2PO4, 25 glucose, 0.5 CaCl2, 7 MgCl2,) using a vibratome (VT1200s,
655 Leica, Germany). Slices containing V1 were isolated and allowed to recover for 30-60 minutes
656 in heated (35°C) carbogenated ACSF (in mM: 125 NaCl, 2.5 KCl, 25 NaHCO3, 1.25 NaH2PO4,
657 25 glucose, 2 CaCl2, 1 MgCl2) before being stored at room temperature.
658 During recordings, slices were perfused with heated (33°C), carbogenated ACSF. Layer 5
659 GCaMP+ cells were patched with borosilicate glass electrodes (4-7MΩ) filled with K-gluconate
660 internal solution (in mM: 130 K-Gluconate, 10 KCl, 2 MgCl2, 10 EGTA, 10 HEPES, 2 Na2-ATP,
661 0.3 Na2-GTP; pH 7.2-74, 290-300 mOsm), containing 0.1 mM Alexa 594 (ThermoFisher, UK)
662 to facilitate visualization of cells. Cellular electrophysiology was recorded using a Multiclamp
663 700B amplifier and associated pCLAMP software (Molecular Devices). Data was acquired at
664 10 kHz and filtered at 3 kHz. For somatic stimulation, 10 current pulses (2-5 ms, 1-1.5nA) were
665 delivered at 5, 10, 25, 50, 100 and 200 Hz. Each pulse was of sufficient amplitude to trigger
666 an action potential. For dendritic stimulation, a monopolar tungsten electrode was placed in
667 L1. Using a constant current stimulator (Digitimer, UK) 10 stimulation pulses (100 µs) were
668 delivered at 5, 10, 25, 50, 100 and 200 Hz at a stimulation intensity sufficient to evoke an
669 action potential. Stimulation was often accompanied by an enhanced afterdepolarization
670 reminiscent of a dendritic spike (Larkum, Kaiser and Sakmann, 1999; Shai *et al.*, 2015). In sham
671 stimulation trials, no stimuli were given.
672 Cells were imaged with a 25x Olympus Objective (1.05 NA; XLPlan N, Olympus) using a two-
673 photon microscope (Femtonics) equipped with a Ti:sapphire pulsing laser (Chameleon Vision-
674 S, Coherent, CA, USA) which was tuned at 920 nm for GCaMP imaging, and 800 nm for Alexa
675 594 imaging. During somatic and dendritic stimulation, xy scans of GCaMP signals at the soma

676 and distal apical dendrite (nexus) were acquired at a rate >120 Hz. Each imaging trial was 6
677 seconds in duration, with stimulation commencing after a 1 s baseline recording.
678 Images were downsampled to 20 Hz and analysed using ImageJ software and custom MATLAB
679 scripts. Electrophysiological traces were analysed using pCLAMP software and custom
680 MATLAB scripts. $\Delta F/F0$ was calculated as: $(F - F0)/(F0 - F_{background})$ where F0 was the mean
681 baseline fluorescent signal during the 1 s baseline recording, and $F_{background}$ was the
682 background fluorescence. F0 in the distal dendrites was often very low, leading to inflated
683 $\Delta F/F0$ values. Consequently, $\Delta F/F0$ signals in the soma and dendrite were standardized to the
684 maximum signal evoked in each compartment. This allowed for fairer comparisons between
685 compartments, and across cells. Calcium transient amplitudes were measured as the peak
686 $\Delta F/F0$ observed within 1 second after the cessation of stimulation. These values were then
687 subtracted by the average peak $\Delta F/F0$ measured in sham stimulation trials. The procedure
688 was repeated for each sham stimulation trial in order to derive a null distribution of peak
689 amplitudes for statistical comparison. Calcium events were also classified as successfully
690 detected if they exceeded 2.8 standard deviations from the expected null, similar to what was
691 used to analyse our *in vivo* data. An event was considered compartment specific if it was
692 detected in one compartment but not in the other.

693 **Statistics**

694 All analysis was performed either using Matlab 2017a, or GraphPad Prism 8. All error bars in
695 the figures represent standard error of the mean (SEM). Statistical tests and independent
696 samples are described in figure legends.
697

698 **Acknowledgments**

699 We thank the GENIE Program and the Janelia Research Campus, specifically V. Jayaraman, R.
700 Kerr, D. Kim, L. Looger, and K. Svoboda, for making GCaMP6 available. We would also like to
701 thank Peter Kind, for allowing access to equipment and reagents required for *ex vivo*
702 experiments. This work was funded by the Wellcome Trust and the Royal Society (Sir Henry
703 Dale fellowship to N.R.), the Marie Curie Actions of the European Union's FP7 program (MC-
704 CIG 631770 to N.R.), the Shirley Foundation, the Patrick Wild Center and the RS MacDonald
705 Charitable Trust Seedcorn Grant (to N.R.), the Simons Initiative for the Developing Brain (to

706 N.R.), the Royal Commission for the Exhibition 1851 (Research Fellowship to Z.P.) and the
707 University of Edinburgh (PhD scholarship to V.F.).

708 Declaration of Interests

709 The authors declare no competing interests

710 References

711 Adam, Y. *et al.* (2019) 'Voltage imaging and optogenetics reveal behaviour- dependent
712 changes in hippocampal dynamics', *Nature*. Springer US. doi: 10.1038/s41586-019-1166-7.

713 Beaulieu-Laroche, L. *et al.* (2019) 'Widespread and Highly Correlated Somato-dendritic
714 Activity in Cortical Layer 5 Neurons', *Neuron*. Elsevier Inc., pp. 1–7. doi:
715 10.1016/j.neuron.2019.05.014.

716 Bittner, K. C. *et al.* (2015) 'Conjunctive input processing drives feature selectivity in
717 hippocampal CA1 neurons', *Nature Neuroscience*, 18(8), pp. 1133–1142. doi:
718 10.1038/nn.4062.

719 Bittner, K. C. *et al.* (2017) 'Behavioral time scale synaptic plasticity underlies CA1 place fields',
720 *Science*, 357(6355), pp. 1033–1036. doi: 10.1126/science.aan3846.

721 Bono, J. and Clopath, C. (2017) 'Modeling somatic and dendritic spike mediated plasticity at
722 the single neuron and network level', *Nature Communications*. Springer US, 8(1), p. 706. doi:
723 10.1038/s41467-017-00740-z.

724 Chavarha, M. *et al.* (2018) 'Fast two-photon volumetric imaging of an improved voltage
725 indicator reveals electrical activity in deeply located neurons in the awake brain', *BioRXiv*.

726 Chen, T.-W. *et al.* (2013) 'Ultrasensitive fluorescent proteins for imaging neuronal activity.',
727 *Nature*, 499, pp. 295–300. doi: 10.1038/nature12354.

728 Cichon, J. and Gan, W.-B. (2015) 'Branch-specific dendritic Ca2+ spikes cause persistent
729 synaptic plasticity', *Nature*, 520(7546), pp. 180–185. doi: 10.1038/nature14251.

730 Dadarlat, M. C. and Stryker, M. P. (2017) 'Locomotion Enhances Neural Encoding of Visual
731 Stimuli in Mouse V1', *The Journal of Neuroscience*, 37(14), pp. 3764–3775. doi:
732 10.1523/JNEUROSCI.2728-16.2017.

733 Erisken, S. *et al.* (2014) 'Effects of Locomotion Extend throughout the Mouse Early Visual
734 System', *Current Biology*. Elsevier Ltd, 24(24), pp. 2899–2907. doi:
735 10.1016/j.cub.2014.10.045.

736 Gerfen, C. R., Economo, M. N. and Chandrashekar, J. (2018) 'Long distance projections of

737 cortical pyramidal neurons', *Journal of neuroscience research*. doi: 10.1002/jnr.23978.

738 Golding, N. L., Staff, N. P. and Spruston, N. (2002) 'Dendritic spikes as a mechanism for
739 cooperative long-term potentiation', *Nature*, 418(6895), pp. 326–331. doi:
740 10.1038/nature00854.

741 Grienberger, C. *et al.* (2017) 'Inhibitory suppression of heterogeneously tuned excitation
742 enhances spatial coding in CA1 place cells', *Nature Neuroscience*, 20(3), pp. 417–426. doi:
743 10.1038/nn.4486.

744 Grienberger, C., Chen, X. and Konnerth, A. (2015) 'Dendritic function in vivo', *Trends in*
745 *Neurosciences*. Elsevier Ltd, 38(1), pp. 45–54. doi: 10.1016/j.tins.2014.11.002.

746 Groh, A. *et al.* (2010) 'Cell-type specific properties of pyramidal neurons in neocortex
747 underlying a layout that is modifiable depending on the cortical area', *Cerebral Cortex*. doi:
748 10.1093/cercor/bhp152.

749 Guerguiev, J., Lillicrap, T. P. and Richards, B. A. (2017) 'Towards deep learning with segregated
750 dendrites', *eLife*, 6, pp. 1–37. doi: 10.7554/eLife.22901.

751 Harris, K. D. and Shepherd, G. M. G. (2015) 'The neocortical circuit: themes and variations',
752 *Nature Neuroscience*, 18(2), pp. 170–181. doi: 10.1038/nn.3917.

753 Helmchen, F. *et al.* (1999) 'In vivo dendritic calcium dynamics in deep-layer cortical pyramidal
754 neurons', *Nature Neuroscience*. doi: 10.1038/14788.

755 Hill, D. N. *et al.* (2013) 'Multibranch activity in basal and tuft dendrites during firing of layer 5
756 cortical neurons in vivo', *Proceedings of the National Academy of Sciences*, 110(33), pp.
757 13618–13623. doi: 10.1073/pnas.1312599110.

758 Hong, Y. K. *et al.* (2018) 'Sensation, movement and learning in the absence of barrel cortex',
759 *Nature*. Springer US, pp. 542–546. doi: 10.1038/s41586-018-0527-y.

760 Kampa, B. M., Letzkus, J. J. and Stuart, G. J. (2006) 'Requirement of dendritic calcium spikes
761 for induction of spike-timing-dependent synaptic plasticity', *The Journal of Physiology*, 574(1),
762 pp. 283–290. doi: 10.1113/jphysiol.2006.111062.

763 Kerlin, A. *et al.* (2018) 'Functional clustering of dendritic activity during decision-making',
764 *bioRxiv*. doi: 10.1101/440396.

765 Kim, E. J. *et al.* (2015) 'Three Types of Cortical Layer 5 Neurons That Differ in Brain-wide
766 Connectivity and Function', *Neuron*. Elsevier Inc., 88(6), pp. 1253–1267. doi:
767 10.1016/j.neuron.2015.11.002.

768 Labarrera, C. *et al.* (2018) 'Adrenergic Modulation Regulates the Dendritic Excitability of Layer
769 5 Pyramidal Neurons In Vivo', *Cell Reports*, 23(4), pp. 1034–1044. doi:
770 10.1016/j.celrep.2018.03.103.

771 Larkum, M. (2013) 'A cellular mechanism for cortical associations: An organizing principle for
772 the cerebral cortex', *Trends in Neurosciences*. Elsevier Ltd, 36(3), pp. 141–151. doi:

10.1016/j.tins.2012.11.006.

Larkum, M. E. *et al.* (2009) 'Synaptic integration in tuft dendrites of layer 5 pyramidal neurons: a new unifying principle', *Science*, 325(5941), pp. 756–760. Available at: http://www.ncbi.nlm.nih.gov/entrez/query.fcgi?cmd=Retrieve&db=PubMed&dopt=Citation&list_uids=19661433.

Larkum, M. E., Kaiser, K. M. and Sakmann, B. (1999) 'Calcium electrogenesis in distal apical dendrites of layer 5 pyramidal cells at a critical frequency of back-propagating action potentials.', *Proceedings of the National Academy of Sciences of the United States of America*, 96(25), pp. 14600–4. doi: 10.1073/pnas.96.25.14600.

Larkum, M. E., Zhu, J. J. and Sakmann, B. (1999) 'A new cellular mechanism for coupling inputs arriving at different cortical layers', *Nature*. doi: 10.1038/18686.

Magee, J. C. and Johnston, D. (1997) 'A synaptically controlled, associative signal for Hebbian plasticity in hippocampal neurons', *Science*. doi: 10.1126/science.275.5297.209.

Manita, S. *et al.* (2015) 'A Top-Down Cortical Circuit for Accurate Sensory Perception', *Neuron*. Elsevier Inc., 86(5), pp. 1304–1316. doi: 10.1016/j.neuron.2015.05.006.

Mazurek, M., Kager, M. and Van Hooser, S. D. (2014) 'Robust quantification of orientation selectivity and direction selectivity', *Frontiers in Neural Circuits*, 8. doi: 10.3389/fncir.2014.00092.

Moore, J. J. *et al.* (2017) 'Dynamics of cortical dendritic membrane potential and spikes in freely behaving rats', *Science*, 355(6331), p. eaaj1497. doi: 10.1126/science.aaj1497.

Naka, A. and Adesnik, H. (2016) 'Inhibitory Circuits in Cortical Layer 5.', *Frontiers in neural circuits*, 10, p. 35. doi: 10.3389/fncir.2016.00035.

Niell, C. M. and Stryker, M. P. (2008) 'Highly selective receptive fields in mouse visual cortex', *J Neurosci*, 28(30), pp. 7520–7536. Available at: http://www.ncbi.nlm.nih.gov/entrez/query.fcgi?cmd=Retrieve&db=PubMed&dopt=Citation&list_uids=18650330.

Pakan, J. *et al.* (2016) 'Behavioral-state modulation of inhibition is context-dependent and cell type specific in mouse visual cortex', *eLife*. Edited by T. D. Mrsic-Flogel. eLife Sciences Publications, Ltd, 5, p. e14985. doi: 10.7554/eLife.14985.

Pakan, J. *et al.* (2018) 'The Impact of Visual Cues, Reward, and Motor Feedback on the Representation of Behaviorally Relevant Spatial Locations in Primary Visual Cortex', *Cell Reports*, 24(10), pp. 2521–2528. doi: 10.1016/j.celrep.2018.08.010.

Pakan, J. M., Francioni, V. and Rochefort, N. L. (2018) 'Action and learning shape the activity of neuronal circuits in the visual cortex', *Current Opinion in Neurobiology*, 52(52), pp. 88–97. doi: 10.1016/j.conb.2018.04.020.

Palmer, L. M. *et al.* (2014) 'NMDA spikes enhance action potential generation during sensory

input.', *Nature neuroscience*. Nature Publishing Group, 17(3), pp. 383–90. doi: 10.1038/nn.3646.

Peters, A. J. *et al.* (2017) 'Reorganization of corticospinal output during motor learning', *Nature Neuroscience*, 20(8), pp. 1133–1141. doi: 10.1038/nn.4596.

Ranganathan, G. N. *et al.* (2018) 'Active dendritic integration and mixed neocortical network representations during an adaptive sensing behavior', *Nature Neuroscience*. Springer US. doi: 10.1038/s41593-018-0254-6.

Remy, S. and Spruston, N. (2007) 'Dendritic spikes induce single-burst long-term potentiation', *Proceedings of the National Academy of Sciences*, 104(43), pp. 17192–17197. doi: 10.1073/pnas.0707919104.

Roome, C. J. and Kuhn, B. (2018) 'Simultaneous dendritic voltage and calcium imaging and somatic recording from Purkinje neurons in awake mice', *Nature Communications*. Springer US, 9(1), p. 3388. doi: 10.1038/s41467-018-05900-3.

Schiller, J. *et al.* (1997) 'Calcium action potentials restricted to distal apical dendrites of rat neocortical pyramidal neurons', *The Journal of Physiology*, 505(3), pp. 605–616. doi: 10.1111/j.1469-7793.1997.605ba.x.

Shai, A. S. *et al.* (2015) 'Physiology of Layer 5 Pyramidal Neurons in Mouse Primary Visual Cortex: Coincidence Detection through Bursting', *PLOS Computational Biology*. Edited by O. Sporns, 11(3), p. e1004090. doi: 10.1371/journal.pcbi.1004090.

Sheffield, M. E. and Dombeck, D. A. (2019) 'Dendritic mechanisms of hippocampal place field formation', *Current Opinion in Neurobiology*. Elsevier Ltd, 54, pp. 1–11. doi: 10.1016/j.conb.2018.07.004.

Sheffield, M. E. J., Adoff, M. D. and Dombeck, D. A. (2017) 'Increased Prevalence of Calcium Transients across the Dendritic Arbor during Place Field Formation', *Neuron*. Elsevier Inc., 96(2), pp. 490-504.e5. doi: 10.1016/j.neuron.2017.09.029.

Silberberg, G. and Markram, H. (2007) 'Disynaptic Inhibition between Neocortical Pyramidal Cells Mediated by Martinotti Cells', *Neuron*, 53(5), pp. 735–746. doi: 10.1016/j.neuron.2007.02.012.

Sjöström, P. J. and Häusser, M. (2006) 'A Cooperative Switch Determines the Sign of Synaptic Plasticity in Distal Dendrites of Neocortical Pyramidal Neurons', *Neuron*, 51(2), pp. 227–238. doi: 10.1016/j.neuron.2006.06.017.

Smith, S. L. *et al.* (2013) 'Dendritic spikes enhance stimulus selectivity in cortical neurons in vivo', *Nature*, 503(7474), pp. 115–120. doi: 10.1038/nature12600.

Spruston, N. *et al.* (1995) 'Activity-dependent action potential invasion and calcium influx into hippocampal CA1 dendrites', *Science*, 268(5208), pp. 297–300. doi: 10.1126/science.7716524.

Stuart, G. J. and Spruston, N. (2015) ‘Dendritic integration: 60 years of progress’, *Nature Neuroscience*, 18(12), pp. 1713–1721. doi: 10.1038/nn.4157.

Stuart, G., Schiller, J. and Sakmann, B. (1997) ‘Action potential initiation and propagation in rat neocortical pyramidal neurons’, *The Journal of Physiology*, 505(3), pp. 617–632. doi: 10.1111/j.1469-7793.1997.617ba.x.

Svoboda, K. *et al.* (1997) ‘In vivo dendritic calcium dynamics in neocortical pyramidal neurons’, *Nature*, 385(6612), pp. 161–165. doi: 10.1038/385161a0.

Takahashi, N. *et al.* (2016) ‘Active cortical dendrites modulate perception’, *Science*, 354(6319), pp. 1587–1590. doi: 10.1126/science.aah6066.

Vetter, P., Roth, A. and Häusser, M. (2001) ‘Propagation of Action Potentials in Dendrites Depends on Dendritic Morphology’, *Journal of Neurophysiology*, 85(2), pp. 926–937. doi: 10.1152/jn.2001.85.2.926.

Vinck, M. *et al.* (2015) ‘Arousal and locomotion make distinct contributions to cortical activity patterns and visual encoding.’, *Neuron*, 86(3), pp. 740–54. doi: 10.1016/j.neuron.2015.03.028.

Waters, J. *et al.* (2003) ‘Supralinear Ca2+ influx into dendritic tufts of layer 2/3 neocortical pyramidal neurons in vitro and in vivo’, *J Neurosci*, 23(24), pp. 8558–8567. Available at: http://www.ncbi.nlm.nih.gov/entrez/query.fcgi?cmd=Retrieve&db=PubMed&dopt=Citation&list_uids=13679425.

Williams, S. R. and Fletcher, L. N. (2019) ‘A Dendritic Substrate for the Cholinergic Control of Neocortical Output Neurons’, *Neuron*. doi: 10.1016/j.neuron.2018.11.035.

Xu, N. *et al.* (2012) ‘Nonlinear dendritic integration of sensory and motor input during an active sensing task.’, *Nature*. Nature Publishing Group, 492(7428), pp. 247–51. doi: 10.1038/nature11601.

Yaeger, C. E., Ringach, D. L. and Trachtenberg, J. T. (2019) ‘Neuromodulatory control of localized dendritic spiking in critical period cortex’, *Nature*. Springer US, pp. 100–104. doi: 10.1038/s41586-019-0963-3.

Young, H. *et al.* (2019) ‘Laminar-specific cortico-cortical loops in mouse visual cortex’, *bioRxiv*. doi: 10.1101/773085.

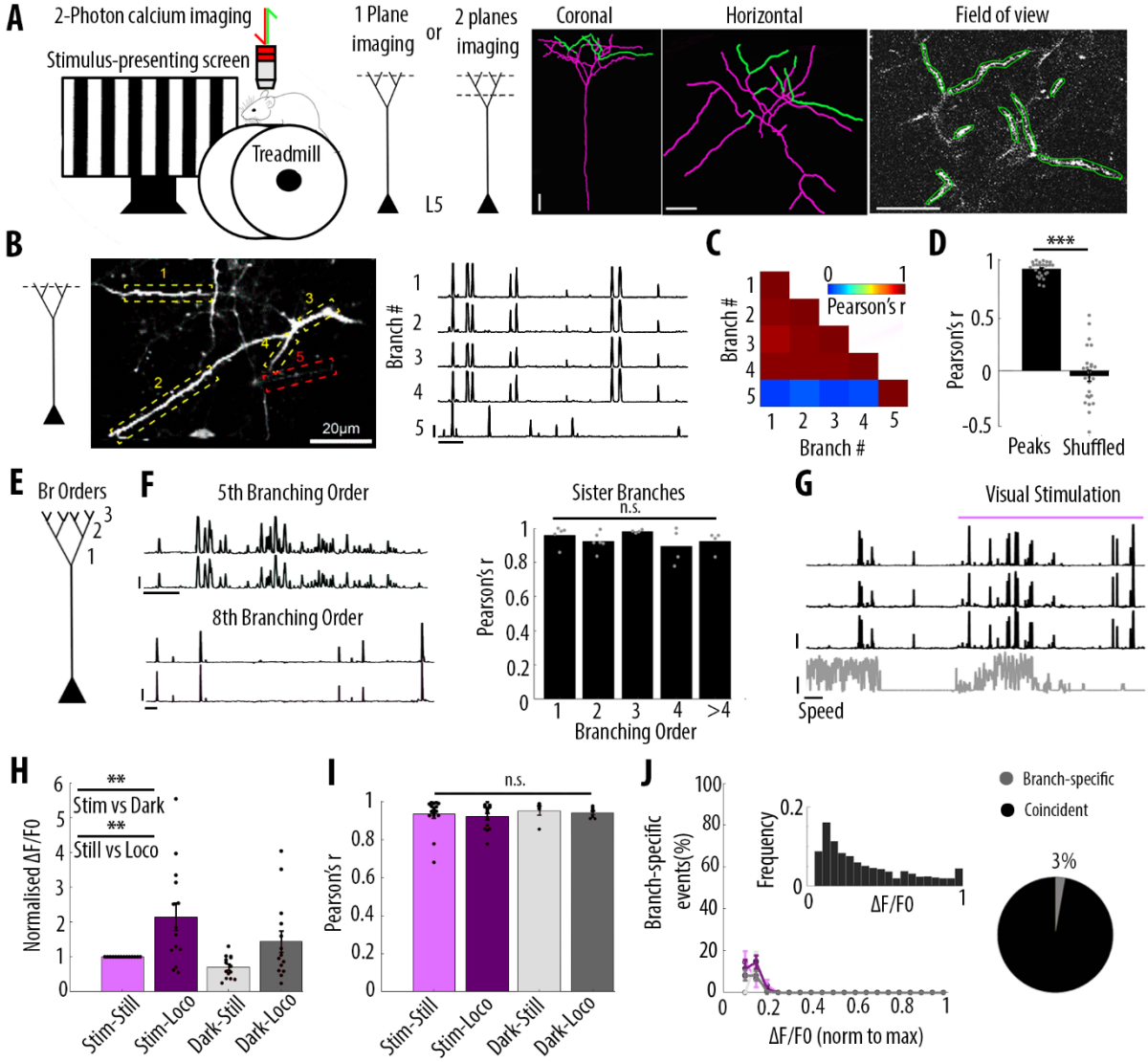

Figure 1. Highly correlated activity in the whole apical tuft of layer 5 pyramidal neurons. **A**) Schematic of the methodological approach. Calcium transients were recorded either in multiple apical tuft dendrites in a single focal plane, or semi-simultaneously in different compartments of individual neurons (Soma, Trunk and Tuft). At the end of each imaging session, a z-stack was recorded for post-hoc reconstruction of each imaged neuron. **B**) Single plane imaging of the apical tuft branches of an individual layer 5 neuron. GCaMP6f-calcium transients of the apical tuft branches belonging to one neuron are shown in traces 1 to 4 while calcium transients of a tuft branch belonging to a different neuron is shown in trace 5. Scale bars, 0.3 ΔF/F0 (normalised to max), 20 s. **C**) Pearson's correlation matrix between the calcium transients of the branches shown in B. Branches that belong to the same neuron (branches 1 to 4, neuron 1) have a mean Pearson's correlation of 0.96, while the branch that belongs to the different neuron (branch 5, neuron 2) has a mean Pearson's correlation value of 0.13 with neuron 1's branches. **D**) Mean Pearson's correlation value between tuft dendrites calcium transient peak amplitudes for each imaged field of view and corresponding shuffled data (Paired t-test, $p = 3.5e^{-15}$; mean = 0.92 and -0.04, sem = 0.01 and 0.05 for branches and shuffled data, respectively; n = 25 fields of view; coming from 14 neurons; 6 animals; 70 branches). **E**) Schematic of the definition of branching orders. **F**) Two representative traces of sibling branches belonging to the 5th and 8th (left panel, labelled) branching order and a quantification of the Pearson's correlation for sibling tuft branches of different

branching orders (right panel). (For 1st, 2nd, 3rd, 4th and more than 4th branching order, One-way ANOVA, p = 0.34; mean = 0.96; 0.92; 0.98; 0.89; 0.92, sem = 0.02; 0.02; 0.01; 0.05; 0.03, n = 5; 6; 4; 4; 4 pairs of branches, respectively). Scale bars, 0.3 ΔF/F0 (normalised to max), 20 s. **G**) Representative traces of 3 tuft branches belonging to the same neuron while the animal was either stationary or running (grey signal, speed) during either darkness or the presentation of drifting grating (purple segment). Scale bars, 12 cm/s, 0.3 ΔF/F0 (normalised to max), 20 s. **H**) Mean ΔF/F0 for apical tuft dendrites during darkness (dark) and visual stimulation (stim) while the animal was either stationary (still) or running (loco). Bar graph is normalised to visual stimulation during stationary condition. Both visual stimulation and locomotion significantly increase the mean ΔF/F0 of tuft branches without any interaction effect (Repeated Measures Two-way ANOVA on log-transformed data, p = 0.005, 0.003 and 0.99 for stim, loco and interaction effects respectively, mean (normalised to stim/still) = 1; 2.15; 0.7; 1.4, sem = 0; 0.38; 0.08 and 0.3, n = 14 neurons). **I**) Pearson's correlation coefficients between tuft dendrites calcium transients of individual neurons during stim-still, stim-loco, dark-still and dark-loco. (Two-way ANOVA, p = 0.43, 0.62 and 0.97 for stim, loco and interaction effects; mean = 0.93; 0.92; 0.95 and 0.94, sem = 0.02; 0.02; 0.02; 0.01, n =16; 14; 5 and 7 fields of views respectively). **J**) Proportion of branch-specific events as a function of GCaMP6f calcium transients' amplitude for the four different conditions (left panel). Neither visual stimulation nor locomotion nor an interaction effect, significantly increased the number of branch-specific events (Three-way ANOVA, p = 0.29; 0.8 and 0.94, respectively; $p < 10^{-15}$ for event amplitude; n= 70 branches from 14 neurons; 6 animals). *Inset*, frequency distribution of the calcium transients' amplitudes detected in the apical tuft branches. *Right panel*, pie chart showing that on average 3% of all calcium transients were detected in only one apical tuft dendritic branch.

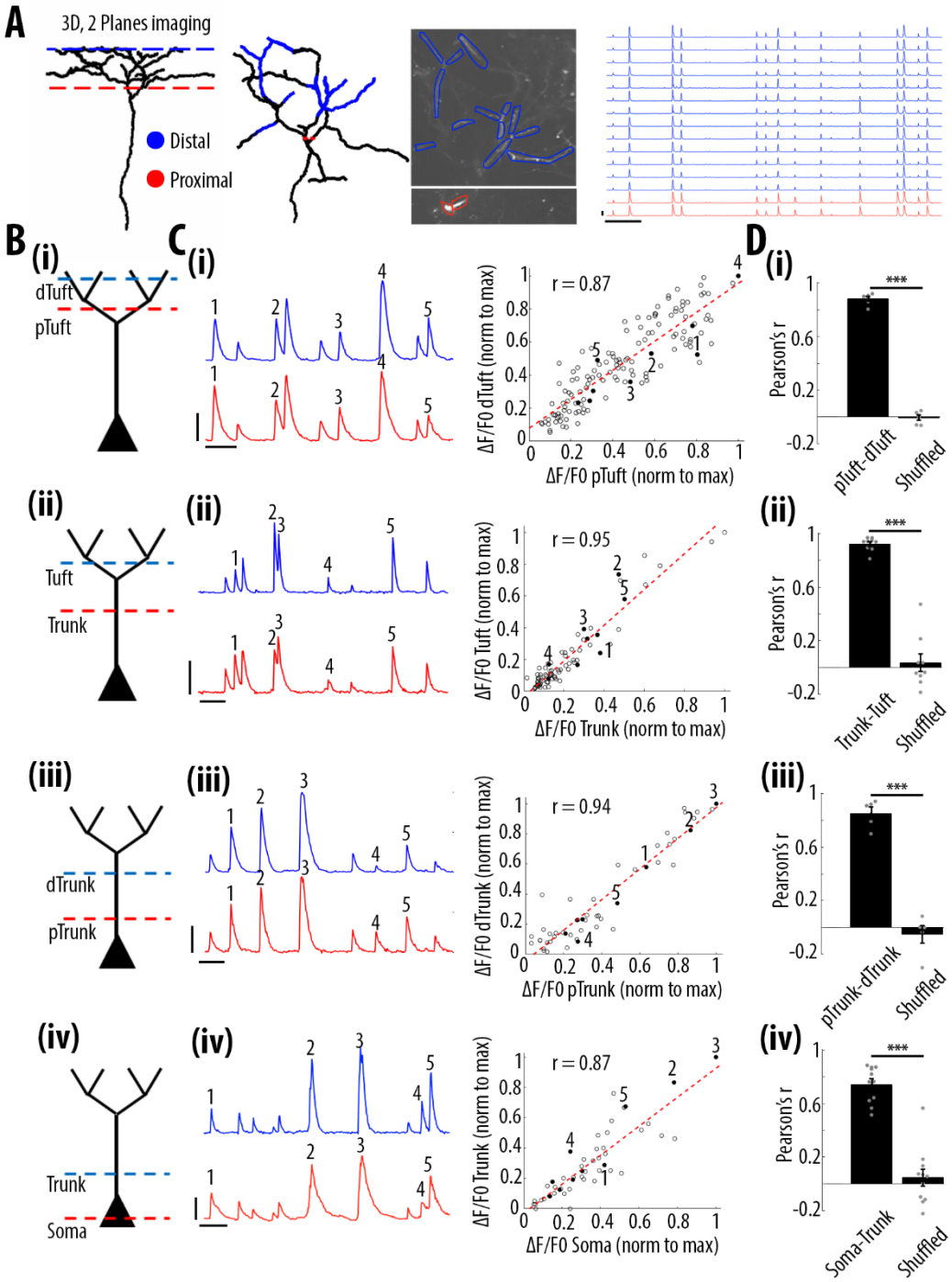
A
3D, 2 Planes imaging
Distal
Proximal
B
(i)
dTuft
pTuft
(ii)
Tuft
Trunk
(iii)
dTrunk
pTrunk
(iv)
Trunk
Soma
C
(i)
r = 0.87
ΔF/F0 dTuft (norm to max)
ΔF/F0 pTuft (norm to max)
(ii)
r = 0.95
ΔF/F0 Tuft (norm to max)
ΔF/F0 Trunk (norm to max)
(iii)
r = 0.94
ΔF/F0 dTrunk (norm to max)
ΔF/F0 pTrunk (norm to max)
(iv)
r = 0.87
ΔF/F0 Trunk (norm to max)
ΔF/F0 Soma (norm to max)
D
(i)
Pearson's r
***
pTuft-dTuft
Shuffled
(ii)
Trunk-Tuft
Shuffled
(iii)
pTrunk-dTrunk
Shuffled
(iv)
Soma-Trunk
Shuffled

916

Figure 2. High correlation of calcium transients between neuronal compartments (soma, trunk, apical tuft) of individual layer 5 neurons. A) Anatomical reconstruction of an individual GCaMP6s-labeled layer 5 pyramidal neuron imaged at two focal planes semi-simultaneously (red dotted lines, proximal; blue, distal). *Left panel*, coronal and horizontal views of the same imaged neuron. *Right panel*, two-photon image of dendritic branches highlighted in red and blue in the horizontal view of the anatomical reconstruction. Example ΔF/F0 traces of highly correlated calcium transients from dendritic branches indicated in red and blue. **B**) Schemata of the compartments imaged semi-simultaneously, (i) proximal tuft-distal tuft, (ii) trunk-tuft, (iii), trunk-trunk, (iv) soma-trunk. pTrunk, dTrunk and pTuft, dTuft indicate proximal and distal portions of the trunk and the apical tuft, respectively. **C**) *Left panel*, representative GCaMP6s-calcium transients imaged in two neuronal compartments semi-simultaneously as shown in B. *Right panel*, scatter plot of peak amplitudes of individual calcium transients in proximal and distal compartments imaged semi-simultaneously, in one example individual neuron. Each dot represents a calcium transient. Peak amplitudes were normalized to the maximum amplitude in each compartment. Filled dots correspond to the transients indicated by numbers in the left panel. Red dotted line indicates the best fit (least square). Pearson's correlation values (r) are indicated for each example pair of neuronal compartment. Scale bars 0.3 ΔF/F0 (normalised to max), 10 s. **D**) Pearson's correlation values for each pair of compartments imaged semi-simultaneously and corresponding shuffled data (Paired t-test, pTuft-dTuft(i), $p = 1.6e^{-6}$, mean = 0.88; -0.01, sem = 0.02; 0.02, n = 6 pairs; Trunk-Tuft(ii), $p = 8e^{-7}$, mean = 0.92; 0.04, sem = 0.02; 0.07, n = 9; pTrunk-dTrunk(iii), $p = 4.4e^{-4}$, mean = 0.85; -0.05, sem = 0.05; 0.07, n = 5; Soma-Trunk(iv), $p = 4.4e^{-6}$, mean = 0.74; 0.05, sem = 0.04; 0.06, n = 11).

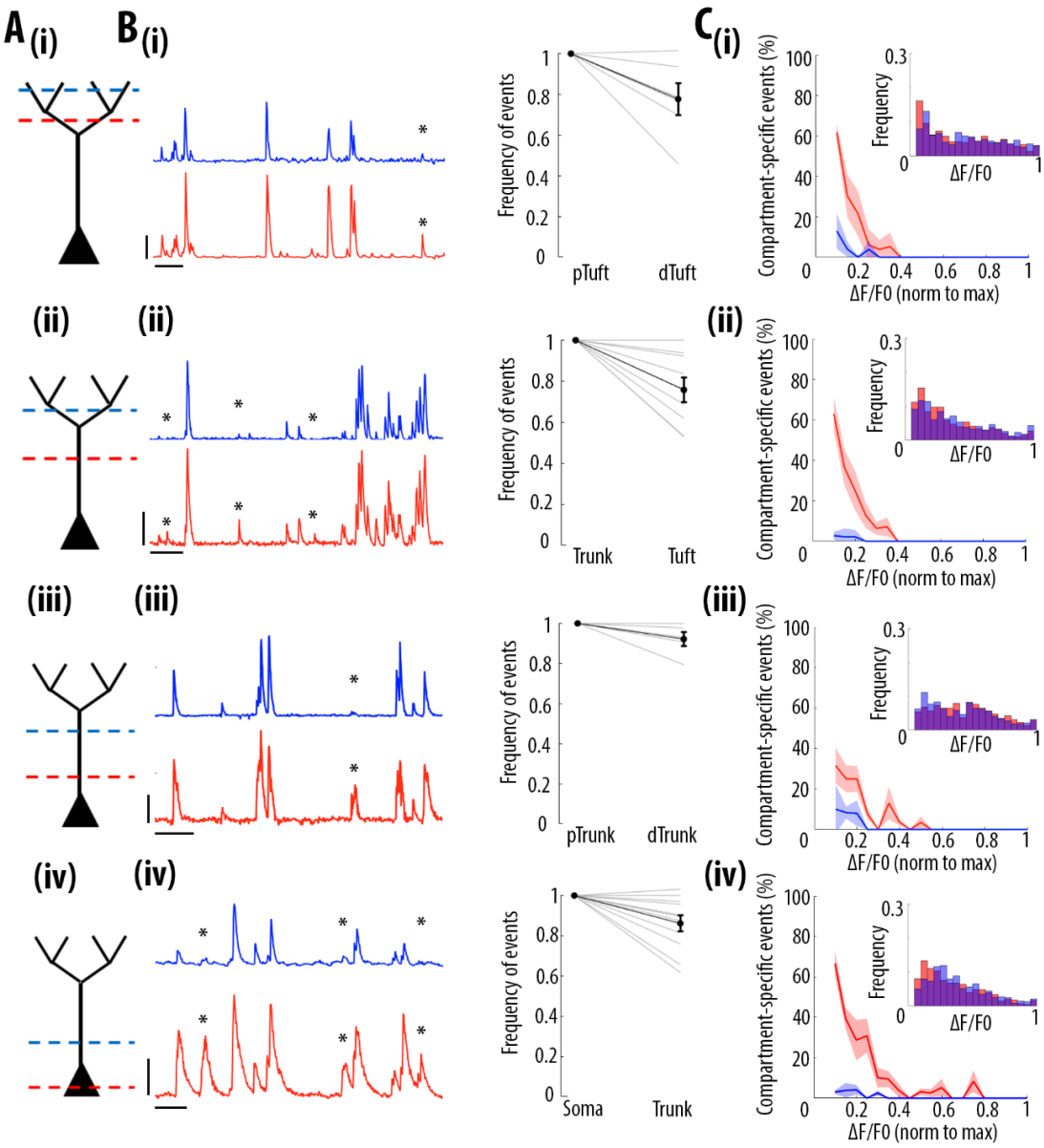

Figure 3. Frequency of calcium transients decreases in a distance and amplitude-dependent dependent manner from the soma to the apical tuft. A) Schemata of the neuronal compartments imaged simultaneously in individual layer 5 neurons. **B**) *Left panel*, representative ΔF/F0 traces of GCaMP6s calcium transients imaged semi-simultaneously in two different compartments as indicated in panel A. Asterisks indicate calcium transients detected in the proximal compartment (red trace) and not detected in the distal one (blue trace). Scale bars 0.25 ΔF/F0 (normalised to max), 20 s. *Right panel*, frequency of detected calcium transients, normalised to the proximal compartment. Individual lines represent individual neurons. Error bar: SEM. **C**) Proportion of compartment-specific events as a function of calcium transients' amplitude. In red, proportion of events only detected in the proximal compartment. In blue, proportion of events only detected in the distal compartment. Thick line represents the weighted mean proportion. Shaded area represents the weighted sem for each bin (0.05). *Upper right panel*, frequency histogram of calcium transient peak amplitudes detected in the proximal (red) and distal (blue) compartments. Peak amplitudes were normalized to the maximum amplitude in each compartment. For all compartments, event amplitude, compartment (proximal vs distal) and an interaction between these two factors significantly affected the proportion of compartment-specific events (Two-way ANOVA, pTuft-dTuft (i), $p < 10^{-15}$, $p = 7.8\times10^{-5}$, $p = 6.2\times10^{-8}$, for event amplitude, proximal versus distal compartment and interaction between amplitude and compartment, respectively, n = 6 pairs; Trunk-Tuft(ii), $p < 10^{-15}$, $p = 3.4\times10^{-9}$, $p < 10^{-15}$, n = 9; pTrunk-dTrunk(iii), $p = 1.3\times10^{-13}$, $p = 2.4\times10^{-4}$, $p = 7\times10^{-3}$, n = 5; Soma-Trunk(iv), $p < 10^{-15}$, $p < 10^{-15}$ and $p < 10^{-15}$, n = 11).

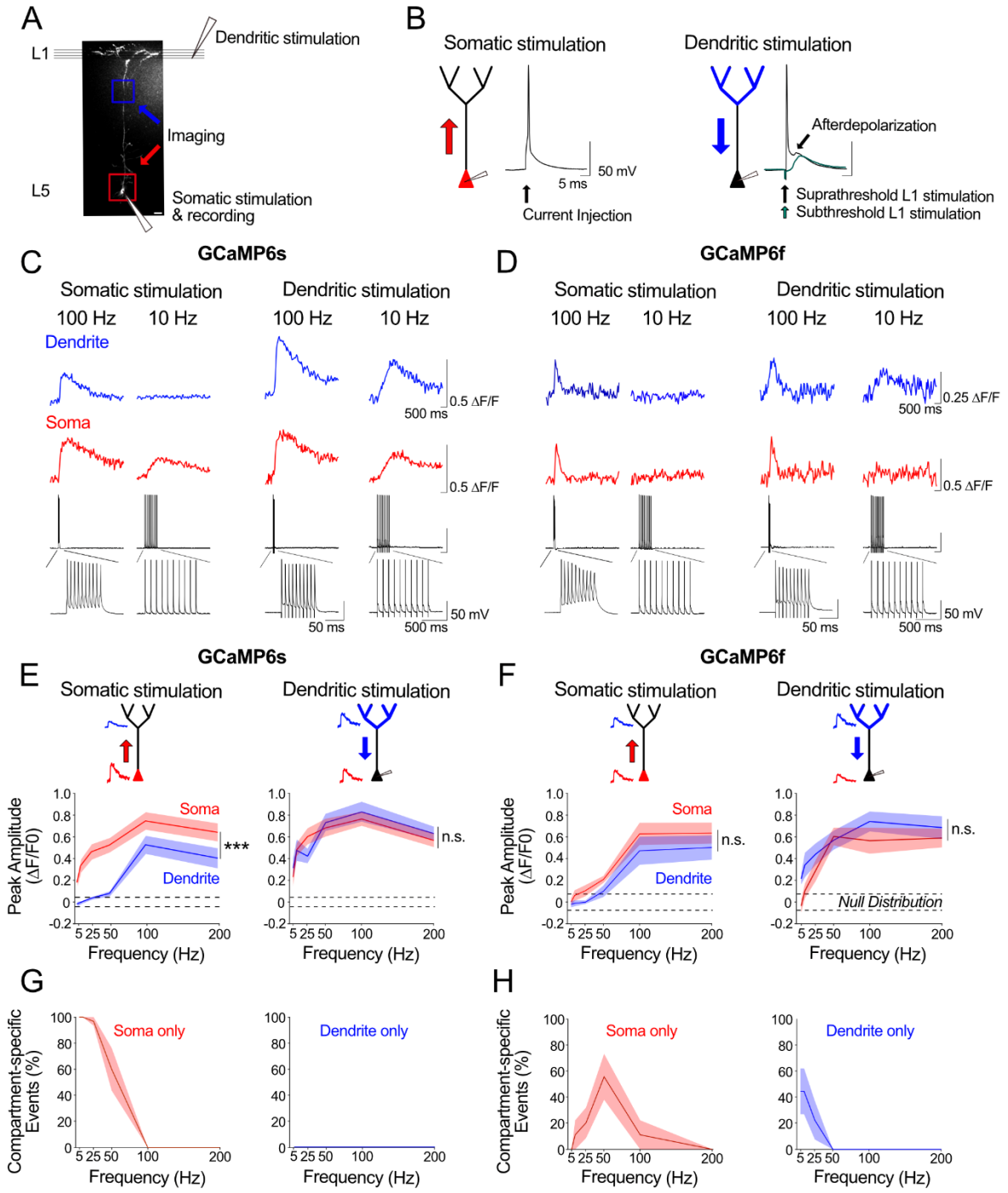

Figure 4. *Ex vivo* calibration of GCaMP6s and GCaMP6f signals in soma and apical tuft dendrites. A) Experimental schemata. Layer 5 pyramidal neurons expressing GCaMP6s or GCaMP6f were recorded using whole-cell patch clamp in acute cortical slices of the primary visual cortex. An example neuron is shown (scale bar = 20 µm). The soma and distal apical dendrite (nexus) were imaged during neuronal spiking, driven either by suprathreshold somatic current injection (somatic stimulation) or layer 1 (L1) stimulation (dendritic stimulation), respectively. Somatic and dendritic stimulation consisted of a train of 10 pulses delivered at 5-200 Hz. **B**) Examples of action potentials driven by somatic and dendritic stimulation. Action potentials triggered by dendritic stimulation were additionally accompanied by an enhanced afterdepolarization reminiscent of a dendritic spike, which had a faster rise time than subthreshold EPSPs and were absent from somatically-evoked action potentials. **C, D**) Example calcium transients imaged in the soma and apical dendrite during somatic and dendritic

stimulation in a L5 neuron expressing GCaMP6s (C) and GCaMP6f (D). Concurrent somatic electrophysiological recordings are shown below each transient. **E, F**) Average peak amplitude of calcium transients recorded in the soma (red) and dendrites (blue) during somatic and dendritic stimulation for GCaMP6s (E) and GCaMP6f (F). Null distribution of peak amplitudes from sham stimulation trials are shown (dashed horizontal lines). **G, H**) Proportion of compartment-specific events detected either in the soma or dendrite during somatic or dendritic stimulation for GCaMP6s (G) and GCaMP6f (H). Shaded areas represent S.E.M. Significance was assessed with two way (E, F) and one way (G, H) repeated measures ANOVA with post-hoc Sidak tests. Asterisks (***) in (E,F) denote factor (soma vs dendrite) significance of $p<0.0001$; n.s. denotes non-significance; significance is not shown for other comparisons but is listed below. For somatic stimulation in (E): soma vs. dendrite: $p<0.0001$ for all frequencies; soma vs. null: $p<0.0001$ for all frequencies; dendrite vs null; $p<0.0001$ for frequencies >50 Hz, $p>0.44$ for frequencies $\leq$ 50 Hz. For dendritic stimulation in (E): soma vs. dendrite: $p>0.11$ for all frequencies; soma vs null: $p<0.0001$ for all frequencies; dendrite vs null: $p<0.0001$ for all frequencies. For somatic stimulation in (F): soma vs. dendrite: $p> 0.49$ for $\geq$ 25 Hz, $p=0.074$ for 10 Hz, $p = 0.054$ for 5Hz; soma vs. null: $p<0.0001$ at $\geq$100 Hz, $p = 0.09$ at 50 Hz, $p>0.7$ at <50 Hz; dendrite vs. null: $p<0.0001$ at $\geq$100 Hz; $p>0.52$ at <50 Hz. For dendritic stimulation in (F): soma vs. dendrite: $p>0.32$ for all frequencies; soma vs. null: $p<0.0001$ at >50 Hz, $p<0.01$ at 25 Hz, $p>0.47$ at <10 Hz; dendrite vs. null: $p<0.0001$ at >25 Hz, $p<0.002$ at 10 Hz, $p=0.11$ at 5 Hz. For somatic stimulation in (G): soma vs null: $p<0.0001$ for $\leq$ 50 Hz, $p>0.44$ for $\geq$ 100 Hz. For dendritic stimulation in (G): dendrite vs null: $p>0.11$ for all frequencies. For somatic stimulation in (H): soma vs null: $p<0.0001$ for 50 Hz; $p>0.12$ for all other frequencies. For dendritic stimulation in (H): dendrite vs null: $p<0.02$ for 5 Hz, $p = 0.10$ for 10 Hz, $p>0.48$ for $\geq$25 Hz. GCaMP6s: n = 10 cells from 4 animals except for 5 Hz stimulation, where n = 5 cells from 3 animals; GCaMP6f: n = 9 cells from 3 animals.

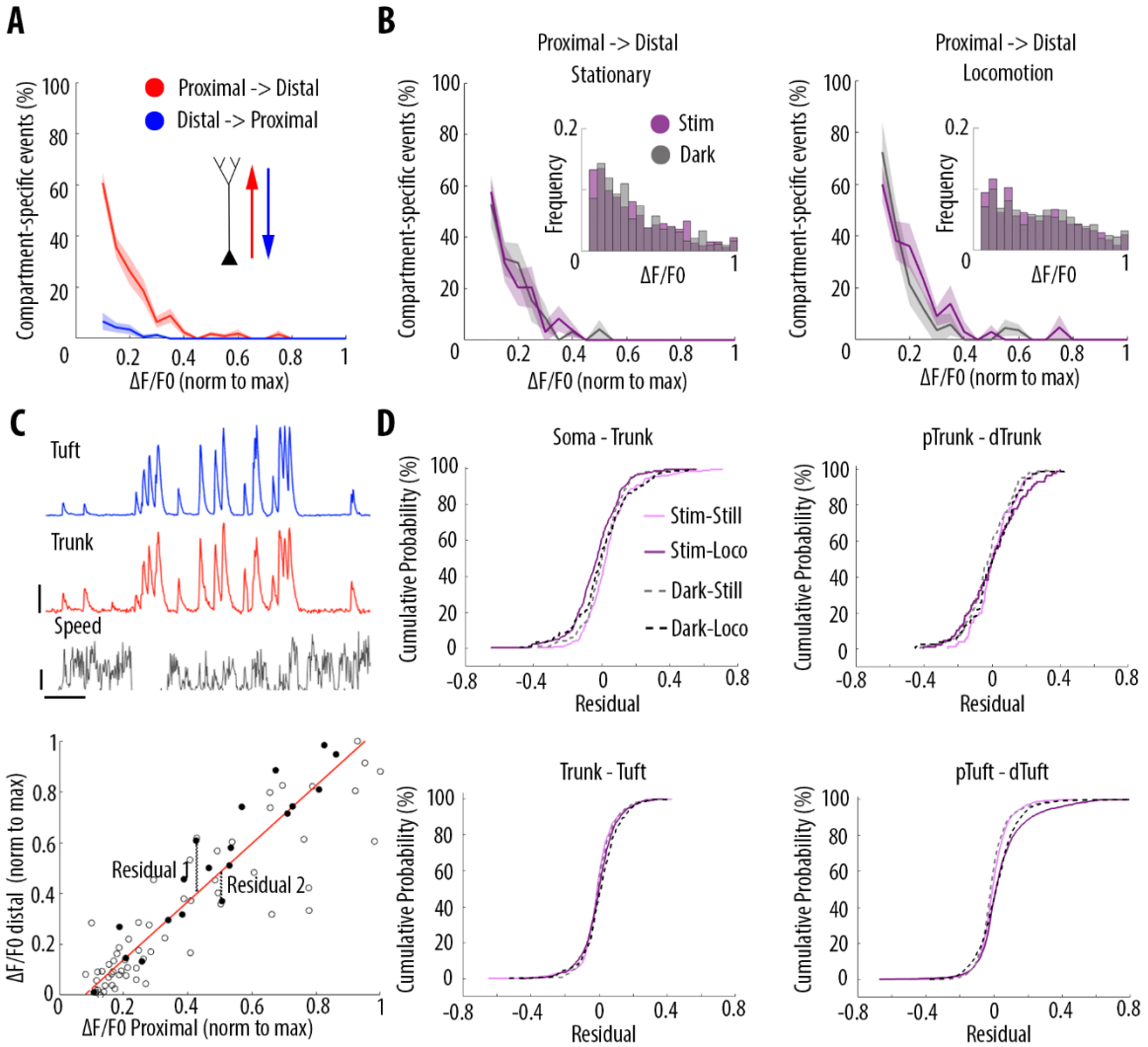

Figure 5. Locomotion and visual stimulation do not alter the relationship between somatic and dendritic calcium transients in layer 5 pyramidal neurons. A) Mean proportion of compartment-specific calcium transients as a function of calcium transient amplitude (average of data points from figure 3C (i-iv)). In red, proportion of events only detected in the proximal compartment. In blue, proportion of events only detected in the distal compartment. Thick line and shaded area: weighted mean and sem for each bin (0.05), respectively. Event amplitude, compartment (proximal vs distal) and an interaction between these two factors significantly affected the proportion of compartment-specific events (Two-way ANOVA, $p < 10^{-15}$, $p < 10^{-15}$, $p < 10^{-15}$, n = 31 pairs of compartments from 19 neurons). **B**) Proportion of compartment-specific events detected in the proximal compartment and not in the distal one, as a function of calcium transient amplitude, during periods of darkness (grey) and visual stimulation with drifting gratings (purple), while the animals were either stationary (left panel) or running (right panel). *Upper right panel*, frequency histogram of calcium transient peak amplitudes detected in proximal compartments during darkness (grey) and visual stimulation (purple). Peak amplitudes were normalized to the maximum amplitude in each compartment. Neither visual stimulation nor locomotion altered the function relating calcium transients amplitude with the proportion of compartment-specific events (Three-way ANOVA, p = 0.69, p = 0.21 and p =

0.64 for visual stimulation, locomotion, and interaction respectively. $p < 10^{-15}$ for event amplitude. No other interaction was found to be statistically significant). **C**) *Upper panel*, example traces of a proximal (trunk, red) and distal (tuft, blue) compartment imaged semi-simultaneously, during stationary and locomotion periods (black trace, speed). Scale bars, 0.25 $\Delta F/F0$ (normalised to max), 12 cm/s, 20 s. *Lower panel*, example of scatter plot of calcium transients' peak amplitudes imaged in a pair of neuronal compartments (trunk-tuft). Each dot represents an individual calcium transient. Filled dots correspond to the transients shown in the upper panel. The red line represents the robust linear regression fit. For each transient, a residual from the robust linear regression was calculated. **D**) Cumulative distributions of the residuals calculated for each pair of compartments and for each condition: visual stimulation (pink, stim), darkness (grey, dark), stationary (still) and locomotion (loco) periods. No significant difference was found between any condition: Three-way ANOVA, $p = 0.96$, $p = 0.23$ and $p = 0.91$ for visual stimulation, locomotion and interaction effect, respectively; $p = 0.86$ for different neuronal compartments No other interaction effect was found to be significant. n = 31 compartments (n = 11 Soma-Trunk; n = 5 pTrunk–dTrunk; n = 9 Trunk–Tuft; n = 6 pTuft-dTuft from 19 neurons).

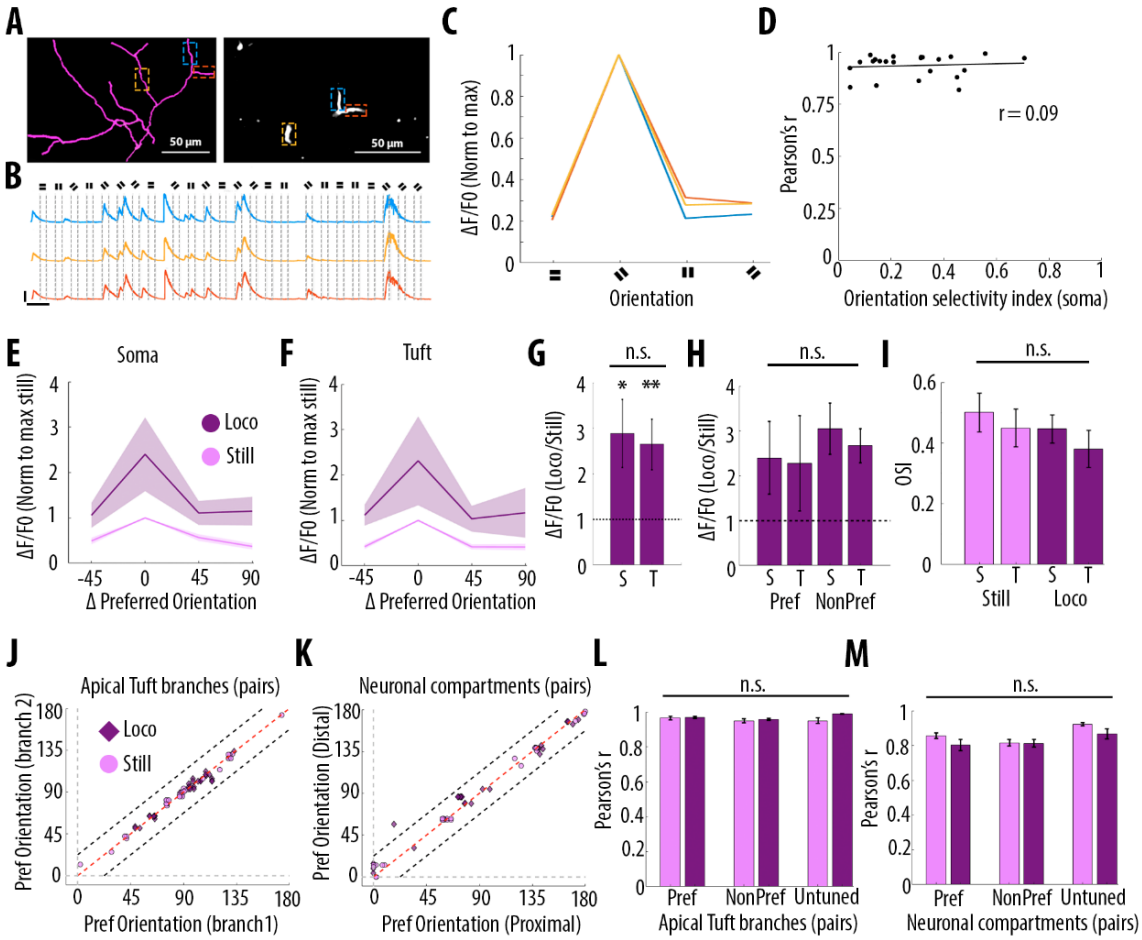

Figure 6. Orientation selectivity does not alter the relationship between somatic and dendritic calcium transients in layer 5 pyramidal neurons. A) Morphological reconstruction (left) and two-photon image (right) of apical tuft branches that were imaged during the presentation of drifting gratings. **B**) Example GCaMP6s calcium transients from the dendritic branches indicated by coloured dashed lines in panel A, during the presentation of drifting gratings of four different orientations. Scale bars 0.3 ΔF/F0 (normalised to max), 10 s. **C**) Tuning curve showing calcium transients amplitudes in response to the 4 grating orientations (average of 24 presentations of each grating, normalised to max), from the 3 branches indicated by coloured dashed lines in panel A. **D**) Mean Pearson's correlation value of all imaged tuft dendritic branches per neuron, as a function of the orientation selectivity of the corresponding soma (each dot corresponds to one neuron; $r^2 = 0.09$, $p = 0.67$, $n = 23$ neurons). The straight black line represents the best fit line (least square). **E**) Tuning curve of somatic calcium signals from orientation selective neurons (somatic OSI > 0.3; n= 15 neurons) during stationary (still, pink) and locomotion (loco, purple) periods. Responses are normalised to the preferred orientation during stationary periods. Thick line and shaded area represent the mean and SEM, respectively. **F**) Same as E, for the corresponding apical tuft branches of the same neurons. For each neuron, responses from all imaged apical tuft branches were averaged (n = 68 apical tuft branches from 15 neurons). **G**) Relative increase in calcium transient amplitudes during locomotion compared to stationary periods both in soma (S) and in corresponding apical tuft dendrites (T), during drifting grating presentations. Locomotion significantly increase responses to drifting gratings both in soma and corresponding apical tuft dendrites (Repeated Measures Two-way ANOVA on log transformed data, $p = 0.02$ and $p = 0.008$ for the effect of locomotion on soma and tuft responses, respectively, n = 15 neurons) without a significant difference between compartments (Paired t-test, $p = 0.38$; mean (normalised to stationary) = 2.89 and 2.65, sem =

0.74 and 0.56; n = 15 soma and 15 apical tufts including 68 branches). **H**) Same as G for responses to the preferred (Pref) and non-preferred (NonPref) orientations (Repeated measures Two-way ANOVA on log-transformed data, p = 0.07, 0.71 and 0.28 for orientation, compartment and interaction effects respectively; mean = 2.4 and 2.28, sem = 0.81 and 1.06 for soma and apical tuft at the preferred orientation; mean = 3.05 and 2.67, sem = 0.57 and 0.38 for soma and apical tuft at the non-preferred orientation; n = 15 soma and 15 apical tufts). **I**) Orientation selectivity index was not significantly different between somatic and corresponding tuft dendrites responses, both during stationary (still) and locomotion (loco) periods (Repeated measures Two-way ANOVA, p = 0.49, p = 0.42 and p = 0.45, for the effects of locomotion, neuronal compartment (soma vs tuft) and interaction, respectively; mean = 0.5; 0.45, sem = 0.06, 0.06 for soma and apical tuft during stationary and mean = 0.45; 0.38, sem = 0.05, 0.06 for soma and apical tuft during locomotion, respectively; n = 15 soma and 15 apical tuft including 68 branches). **J**) Scatter plot of the preferred orientation in pairs of apical tuft branches belonging to the same neuron and imaged simultaneously, during stationary (pink circles) and locomotion (purple diamonds) periods (n = 31 pairs). Dashed red line: identity line; Dashed black lines: identity +/- 22.5 degrees in vectoral space. **K**) Same as J for pairs of neuronal compartments imaged simultaneously. n = 33 pairs. **L**) Pearson's correlation of calcium transients between pairs of apical tuft branches belonging to the same orientation-selective neuron, during the presentation of the preferred (Pref) and non-preferred (NonPref) grating orientations, both during stationary (pink) and locomotion (purple) periods (n = 31 pairs). Correlation values from branches belonging to non-selective neurons (OSI < 0.3, untuned), during the presentation of all oriented gratings, are shown on the right columns (n= 10 pairs). Neither gratings orientation nor locomotion significantly affected the correlation between pairs of branches (Two-way ANOVA, p = 0.20, p = 0.07 and 0.38 for orientation, locomotion and interaction effect, respectively). **M**) Same as L, for different neuronal compartments (Two-way ANOVA, p = 0.27, p = 0.09 and 0.43 for orientation, locomotion and interaction effect, respectively; n = 33 pairs for Pref, NonPref and 36 pairs for untuned). Error bars: SEM.

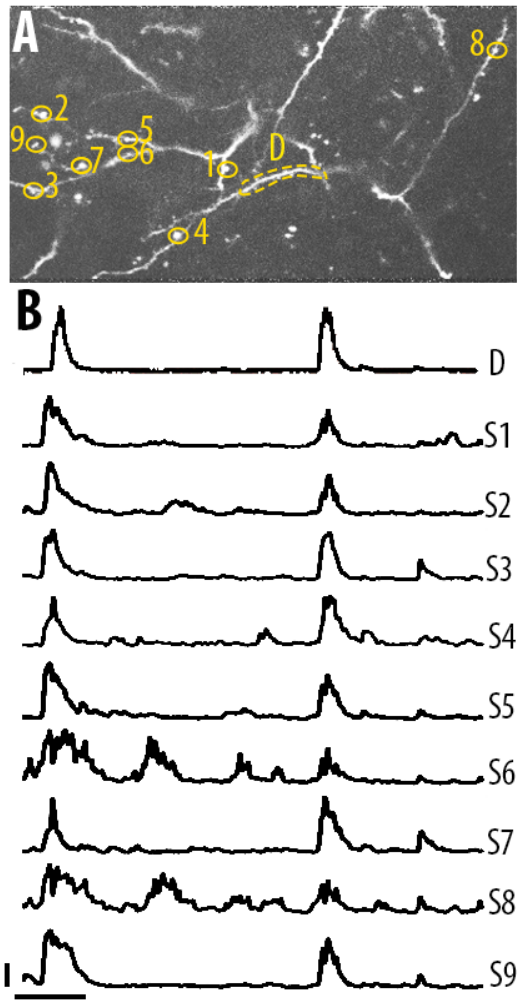

Figure 1- figure supplement 1. Single spine calcium transients in the apical tuft dendrites of layer 5 neurons. A) Two-photon image of an example field of view showing the apical tuft branches of an individual GCaMP6-labelled layer 5 neuron. **B**) Example ΔF/F0 traces for the individual spines shown in panel A. Error bars indicate 0.3 ΔF/F0 (normalised to max), 10 s.

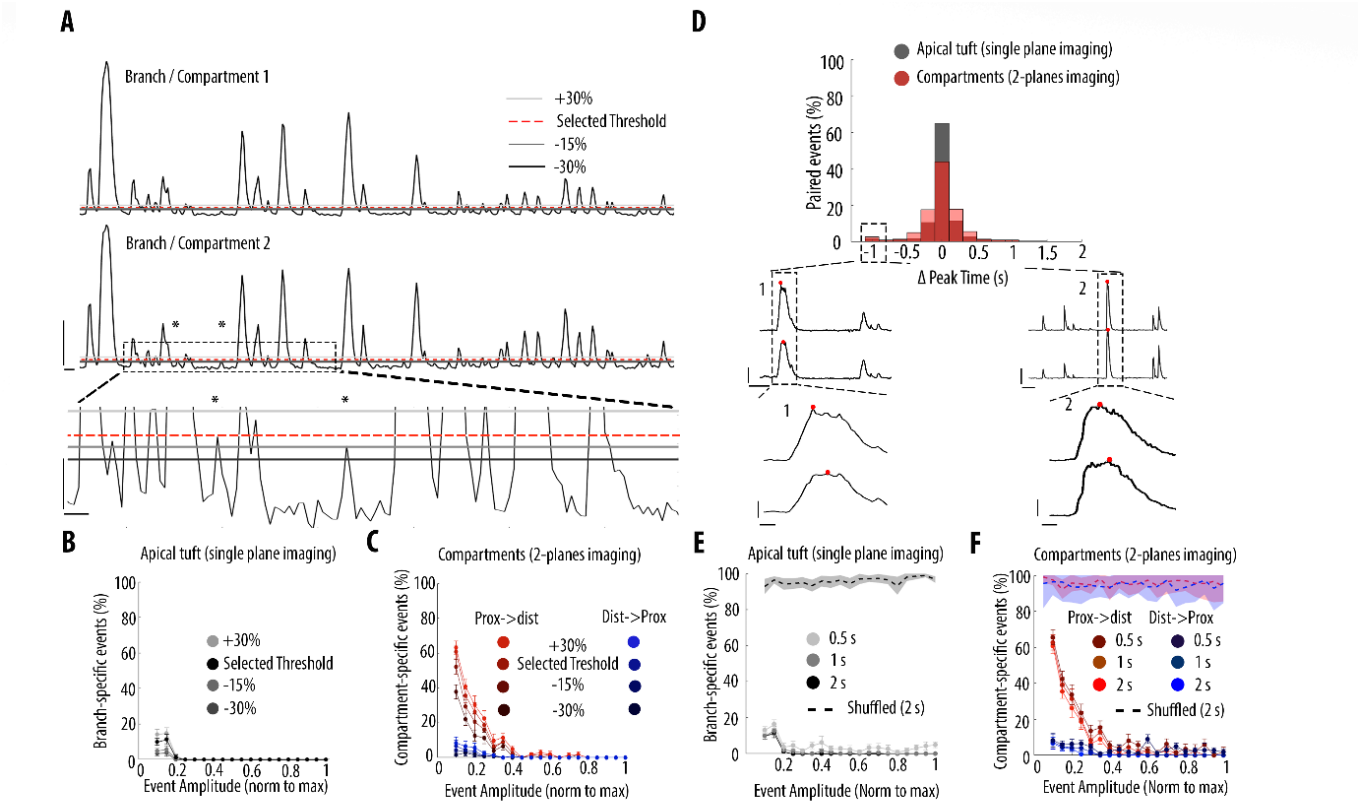

Figure 1- figure supplement 2. Impact of different thresholds and coincident windows on the quantification of branch-specific and compartment-specific events. A) Example ΔF/F0 traces of two sibling branches in the apical tuft branches of an individual layer 5 pyramidal neuron. Asterisks indicate two calcium transients which were not detected using the selected threshold for peak amplitude but were detected lowering the threshold by 30%. *Lower panel*, zoomed image of the dotted area in the middle panel. To assess the resilience of our results to different thresholds, we assessed the proportion of branch/compartment specific events, keeping the selected threshold constant in one branch/compartment (red-dotted line) and varying the threshold in the second branch/compartment from +30% to -30% (light, medium and dark grey lines, respectively). Scale bars: upper panel, 0.3 ΔF/F0 (normalised to max), 5 s; lower panel: 0.03 ΔF/F0, 1s. **B**) Proportion of apical tuft branch-specific events as a function of calcium transients' amplitude, detected with different thresholds. **C**) Proportion of compartment-specific events as a function of calcium transients' amplitude, detected with different thresholds. Same colour code as in Figure 3. **D)** Distribution of time intervals between peaks of calcium transients detected as coincident. Black, distribution for apical tuft events. Red, distribution for pairs of neuronal compartments (2-planes imaging). *Lower panel,* Examples of cases with the largest time interval between two coincident events (offset by 1 second) (dashed rectangle in D). Lower traces: zoomed view of the dashed area 1 and 2. The red dot indicates the frame at which a peak was detected for each pair of compartment. Scale bars: 0.3 ΔF/F0 (normalised to max), 10s (upper panel) and 1s (lower panel). **E)** Proportion of branch-specific events as a function of calcium transients' amplitude using different time windows (0.5s, 1s and 2s) to define coincidence. The dashed line represents the proportion of branch-specific events obtained from shuffled ΔF/F0 signals, with the selected time window (2 s). **F)** Same as in E, for compartment-specific events. Same colour code as Figure 3.

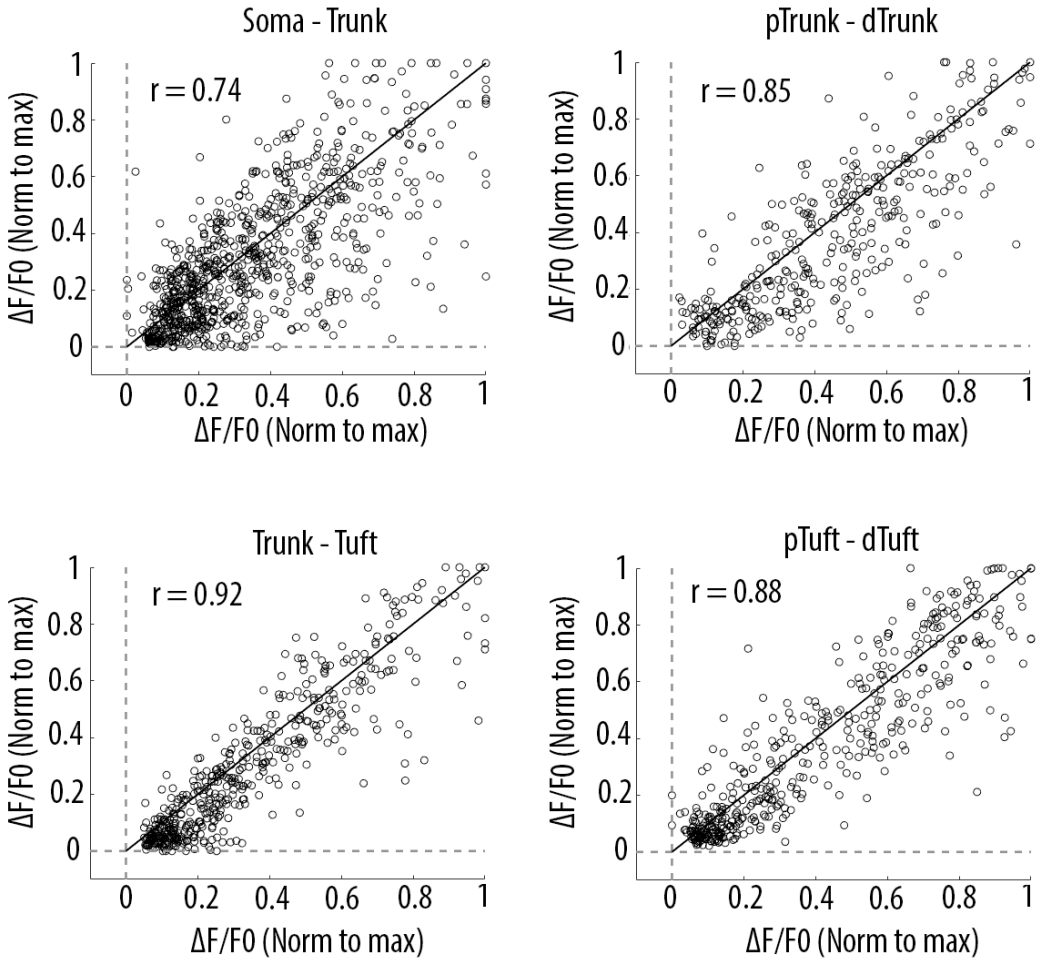

Figure 2- figure supplement 1. Scatter plots of peak amplitudes of individual calcium transients in all proximal and distal compartments imaged semi-simultaneously. Each dot represents a calcium transient. Peak amplitudes were normalized to the maximum amplitude in each compartment. x-axis: proximal compartment; y-axis: distal compartment. Black line indicates the identity line. The mean Pearson's correlation values (r) calculated per neuron, as reported in figure 2D (i-iv), are indicated for each pair of compartment. Soma-Trunk, n = 858 transients from 11 neurons; pTrunk-dTrunk, n = 360 transients from 5 neurons; Trunk-Tuft, n = 479 transients from 9 neurons; pTuft-dTuft, n = 447 transients from 6 neurons; For visualization purpose, for Trunk-Tuft and pTuft-dTuft, only transients from one pair of imaged compartments are shown per neuron.

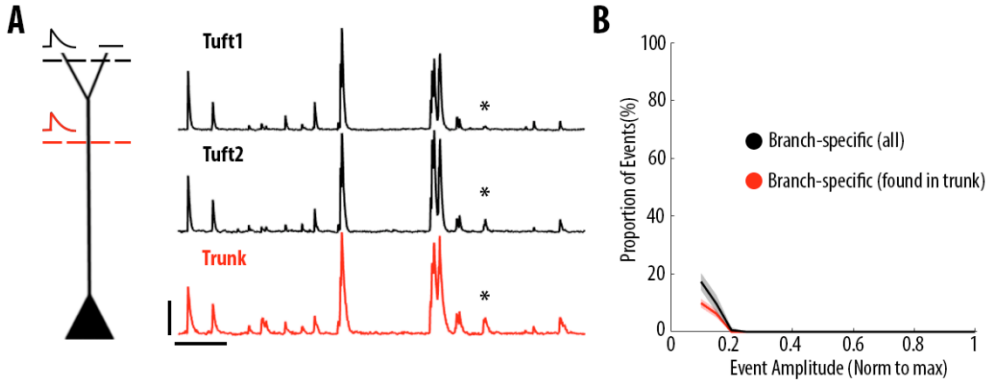

Figure 2- figure supplement 2. Most dendritic events detected as branch-specific were also detected in the trunk. A) Example ΔF/F0 traces of GCaMP6s calcium transients imaged semi-simultaneously in the trunk (red) and in two sibling apical tuft branches (black) of an individual layer 5 neuron. The asterisks indicate a calcium transient that was only detected in one of the two apical tuft branches (tuft 2) and thus classified as a branch-specific event. This transient was also detected in the trunk of the same neuron. Scale bars 0.25 ΔF/F0 (normalised to max), 20 s. **B)** Proportion of apical tuft dendritic branch-specific events, as a function of GCaMP6s calcium transient amplitude. Black, all apical tuft dendrites events detected as branch-specific. Red, proportion of branch-specific events which were also simultaneously detected in the corresponding trunk. On average, 60% of branch-specific events were also found in the trunk.

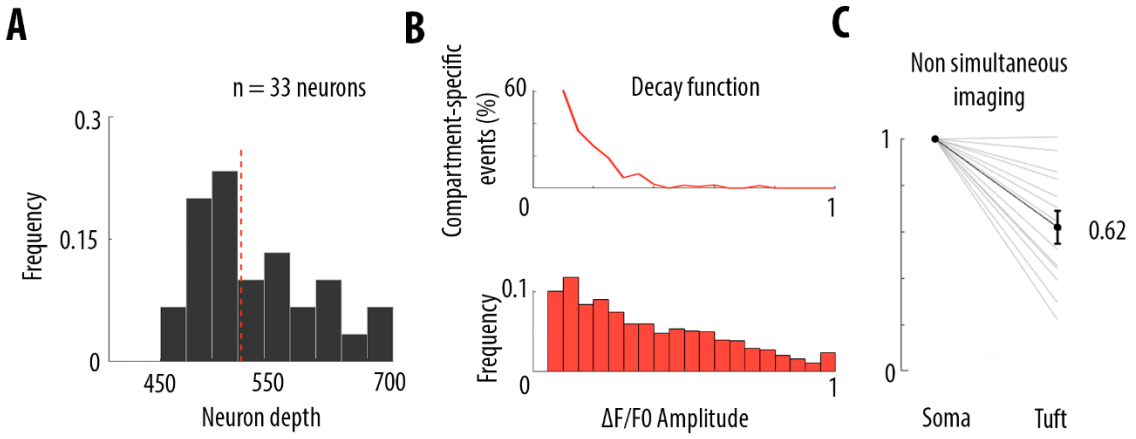

Figure 3-figure supplement 1. Frequency decrease of calcium transients from soma to apical tuft. A) Histogram distribution of the depths at which somata from neurons included in this study have been imaged. The red dotted line indicates the median (528 µm from the dura). **B**) Estimation of the proportion of somatic calcium events not detected in the distal part of the apical tuft, for the data set in which pairs of compartments were imaged semi-simultaneously (Figure 3). Pairs of compartments (soma-trunk, trunk-trunk, trunk-tuft, tuft-tuft) were imaged at a distance of 170 µm (see Methods). As a consequence, the average amplitude-dependent decay function of compartment-specific events (top panel, same as figure 5A) represents the decay function within 170 µm. We projected the decay measured within 170 µm, to the distance between each soma and distal apical tuft, estimated by the depth of the soma from the dura (panel A). We multiplied the amplitude-dependent decay function by the corresponding scaling factor and we applied this scaled function to the frequency distribution of calcium transient amplitudes (lower panel) at each bin (0.05 ΔF/F0). The frequency distribution was derived by averaging all the calcium events in all proximal compartments (see distribution of event amplitudes for each proximal compartment in red in figure 3). Using this approach, we calculated that the proportion of somatic events that were not detected in the tuft was 39% (61% of coincident events). **C**) Frequency of detected calcium transients in the apical tuft, normalised to the frequency of transients in the corresponding soma, for neurons in which both compartments were imaged non-simultaneously. Individual lines represent individual neurons (n=13 neurons). Error bar: SEM.

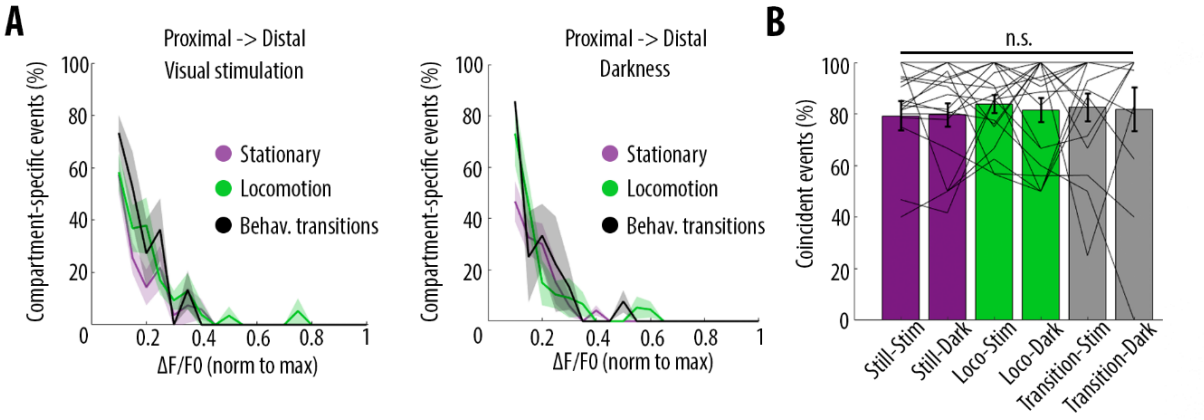

Figure 5- figure supplement 1. Behavioural-state transitions between stationary and locomotion do not alter the relationship between somatic and dendritic calcium transients. **A**) Proportion of compartment-specific events detected in the proximal compartment and not in the distal one, as a function of calcium transient amplitude, during periods of visual stimulation (left panel) and darkness (right panel), while the animals were either stationary (pink), running (green) or in transition between stationary and running (black). Periods of transition were excluded from stationary and locomotion periods. No significant difference was found between any condition (Three-way ANOVA, $p = 0.32$, $p = 0.42$ and $p = 0.64$ for visual stimulation, behavioural state, and interaction respectively; $p < 10\text{-}15$ for event amplitude; no other interaction was found to be statistically significant, $n = 31$ pairs of compartments from 19 neurons). **B**) Proportion of coincident calcium transients in proximal and distal compartments imaged semi-simultaneously during the different behavioural conditions: visual stimulation (stim), darkness (dark), stationary (still), locomotion (loco) and transitions between stationary and locomotion (transition) periods. Each data point corresponds to one neuron (n= 19 neurons). No significant difference was found across conditions (Two-way ANOVA on log-transformed data, $p = 0.93$, $p = 0.87$ and $p = 0.51$ for visual stimulation, behavioural state and interaction effects, respectively).

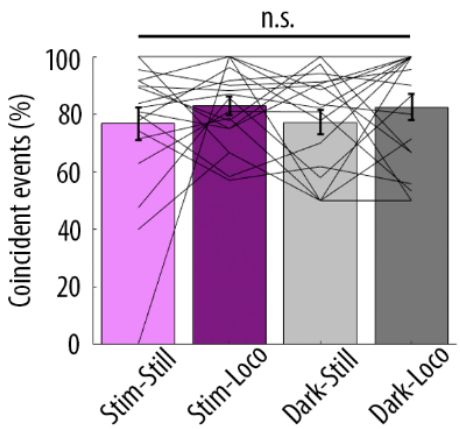

Figure 5- figure supplement 2. Proportion of coincident calcium transients in proximal and distal compartments imaged semi-simultaneously during the different behavioural conditions: visual stimulation (stim), darkness (dark), stationary (still) and locomotion (loco) periods. Each data point corresponds to one neuron (n= 19 neurons). No significant difference was found across conditions (Repeated Measures Two-way ANOVA on log-transformed data, $p = 0.43$, $p = 0.29$ and $p = 0.35$ for visual stimulation, locomotion and interaction effects, respectively).